ANALYSIS OF SLEWING
AND ATTITUDE DETERMINATION
REQUIREMENTS FOR CTEx

THESIS

William J. Starr, Jr., Major, USA

AFIT/GSS/ENY/10-M05

DEPARTMENT OF THE AIR FORCE
AIR UNIVERSITY

AIR FORCE INSTITUTE OF TECHNOLOGY

Wright-Patterson Air Force Base, Ohio

AFIT/GSS/ENY/10-M05

ANALYSIS OF SLEWING
AND ATTITUDE DETERMINATION
REQUIREMENTS FOR CTEx

THESIS

Presented to the Faculty

Department of Aeronautics and Astronautics

Graduate School of Engineering and Management

Air Force Institute of Technology

Air University

Air Education and Training Command

In Partial Fulfillment of the Requirements for the

Degree of Master of Science (Space Systems)

William J. Starr, Jr., BS

Major, USA

March 2010

APPROVED FOR PUBLIC RELEASE; DISTRIBUTION UNLIMITED.

AFIT/GSS/ENY/10-M05

ANALYSIS OF SLEWING
AND ATTITUDE DETERMINATION
REQUIREMENTS FOR CTEx

William J. Starr, Jr., BS

Major, USA

Approved:

//signed//   12 Mar 2010
_____   _____
Jonathan T. Black (Chairman)   Date

//signed//   12 Mar 2010
_____   _____
Carl R. Hartsfield (Member)   Date

//signed//   12 Mar 2010
_____   _____
Ronald J. Simmons (Member)   Date

AFIT/GSS/ENY/10-M05

Abstract

This thesis examines the slewing and attitude determination requirements for the Chromotomographic Experiment (CTEX), a chromotomographic-based hyperspectral imager, to be mounted on-board the Japanese Experiment Module (JEM) External Facility (EF). The in-track slewing requirement is driven by the facts that CTEx has a very small field of view (FOV) and is required to collect 10 seconds of data for any given collection window. The need to slew in the cross-track direction is a product of the small FOV and target/calibration site access. CTEx incorporates a two-axis slow-steering dwell mirror with a range of +/- 8 degrees and an accuracy of 10 arcseconds in each axis to slew the FOV. The inherent inaccuracy in the knowledge of the International Space Station's (ISS) attitude (+/- 3 degrees) poses significant complications in accurately pointing CTEx even with more accurate (0.3 degrees) attitude information provided by the JEM. The desire is for CTEx to incorporate a star tracker with 1 arcsecond accuracy to determine attitude without reliance on outside sources.

Table of Contents

List of Figures

List of Tables

ANALYSIS OF SLEWING
AND ATTITUDE DETERMINATION
REQUIREMENTS FOR CTEx

I. Introduction

This thesis will present an engineering analysis of pointing and tracking require-
ments for the Space Chromotomographic Experiment (CTEx) to be flown aboard the
International Space Station (ISS) as well as an overview of the mission plan for CTEx.
CTEx is an experiment comprised of three phases: a laboratory-based experiment, a
ground-based experiment, a space-flight experiment. CTEx is currently in the ground-
based experiment phase at a technology readiness level (TRL) of three. Successful com-
pletion of the space-flight experiment will raise the TRL for space-based hyperspectral
chromotomographic imaging to six.[4]

The objective of the analysis is to determine requirements for both along track and
cross track pointing and tracking. The biggest concerns are the attitude accuracy of the
ISS and the inherent pointing accuracy of the telescope that RC Optical Systems, Inc.
of Flagstaff, Arizona is building.

1.1   Spectroscopy

Spectroscopy has been around since 1666 when Sir Isaac Newton showed that light
from the sun could be dispersed into a continuous set of colors.[5] Generally speaking,
spectroscopy is the science that is "concerned with the theory and interpretation of
spectra"[6]. The spectra of concern can fall anywhere within the electromagnetic spec-
trum, depicted in Figure 1.1. These spectra are unique to individual molecules and are
produced by transmission, emission, absorption, and reflection. The spectra produced
can be used as a fingerprint since emission and absorption can only occur at well-defined
frequencies for a given molecule.[7] Emission spectra can be classified as line, band, or
continuous. The first two are discontinuous and result in a spectra of bright lines or
bands at certain frequencies and dark lines or bands at all other frequencies.[6] Figure

1.2 is an example of line emission spectra for several elements. The unique combinations of these lines let you characterize specific compounds in combustion events.

THE ELECTRO MAGNETIC SPECTRUM
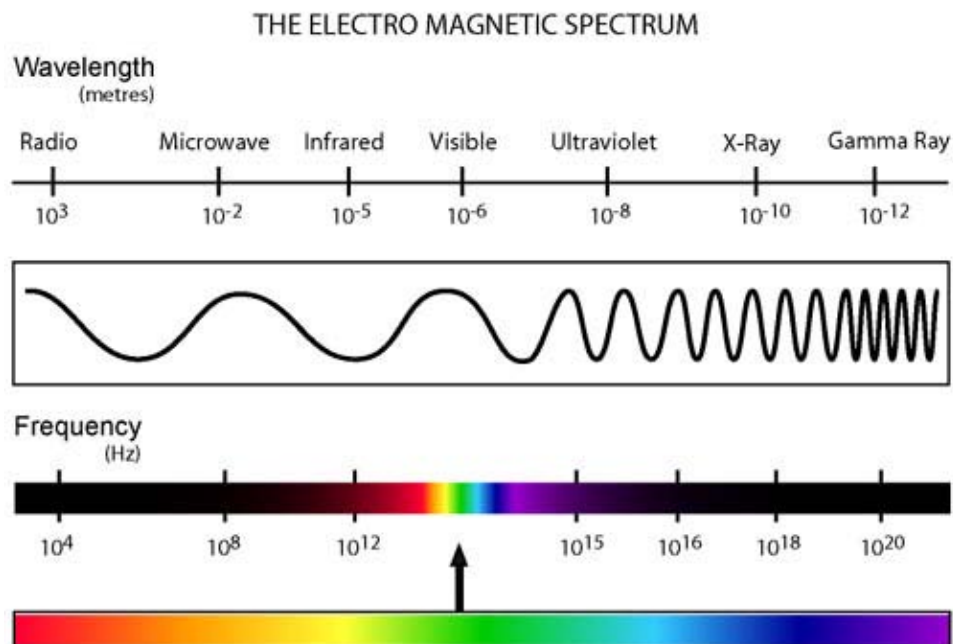
Figure 1.1:   Electromagnetic Spectrum[8]

Imaging spectroscopy is a field that creates an image through the dispersion and collection of many different bands of light. Specifically, this field takes the resulting spectral signature and correlates the spectra spatially to pixels on the imager which creates an image. The number and width of the bands provides the distinction between panchromatic, mulitspectral, hyperspectral, and ultraspectral. Although there is no universal definition of these terms, Table 1.1 depicts an accepted definition. The progression toward hyperspectral and ultraspectral is important when trying to derive the composition of a scene.

Table 1.1:   Spectral Sensing Terminology[10]

	Number of Bands	Width of Bands (μm)
PANCHROMATIC	1	0.5-2.0
MULTISPECTRAL	2-30	0.06-0.2
HYPERSPECTRAL	30-400	$\approx$0.01
ULTRASPECTRAL	>400	$\approx$0.001
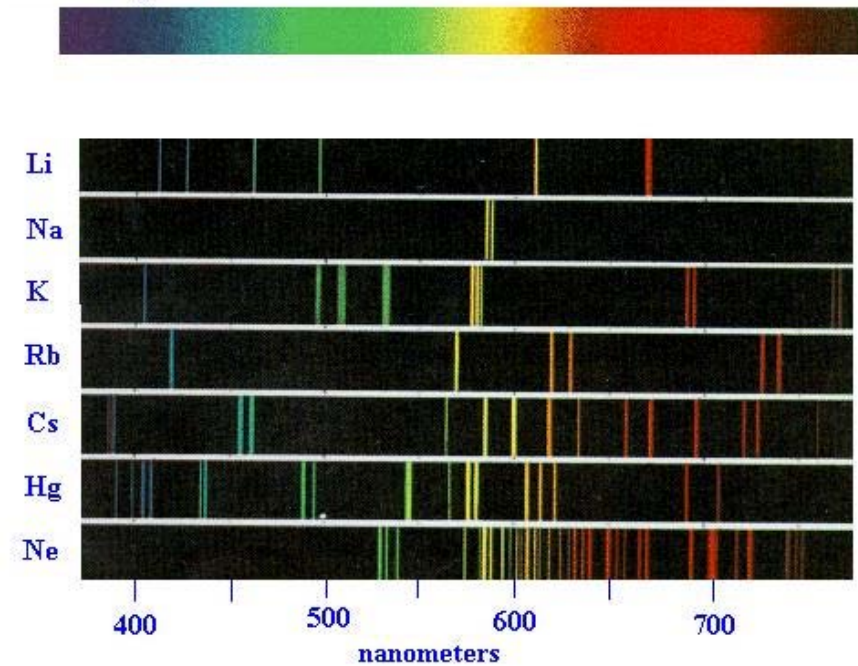
Figure 1.2:   Line Emission Spectra[9]

The dramatic difference between multispectral and hyperspectral imaging is depicted in Figure 1.3. Each pixel in the hyperspectral scene has a continuous spectrum. The continuous spectrum provides greater resolution, showing changes across the range of wavelengths not just at specific locations. The increased resolution enhances the ability to distinguish the material in the scene from similar materials.

The generation of hyperspectral data results in several advantages over multispectral imaging; however, this increased resolution results in an increase in required data processing and transmission. The list of benefits include:

- Hyperspectral imaging improves target detection and identification.

  - Increasing the number of bands increases the probability of distinguishing a target from the background while reducing the number of false alarms.

  - The identification of many materials requires higher spectral resolution than multispectral imaging provides.

3
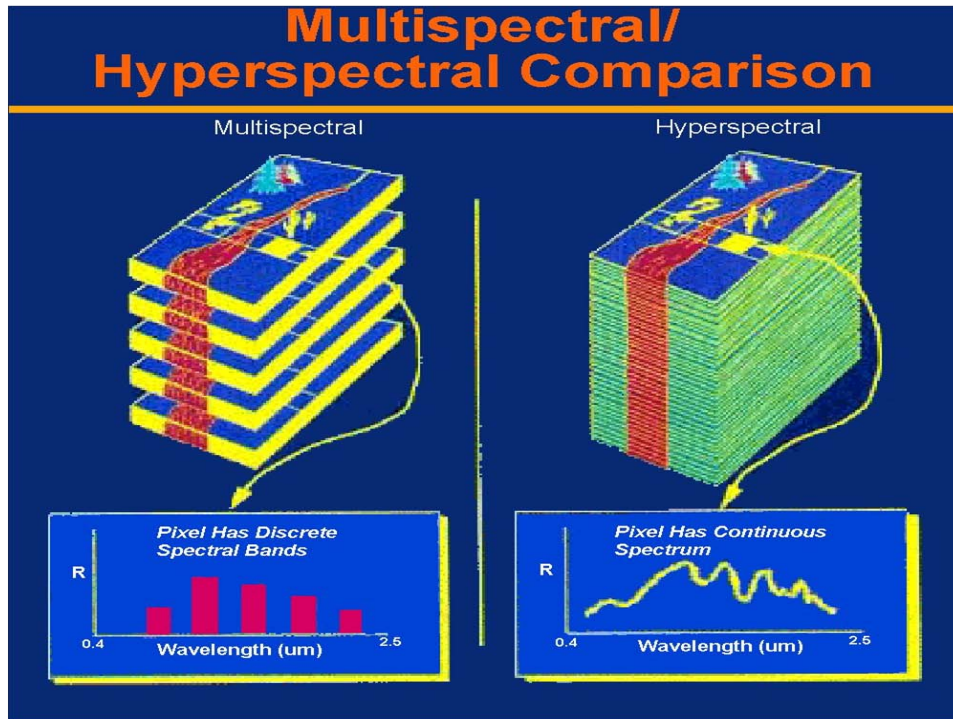
Figure 1.3:   Multispectral and Hyperspectral Data Cube Comparison[10]

- Hyperspectral imaging has higher versatility and flexibility.

    - Hyperspectral imaging covers the entire spectrum of design continuously. Consequently, any combination of bands can be analyzed by a single sensor.

    - There is often incomplete knowledge of a target's composition. The continuous spectrum allows the exploitation of potentially unknown characteristics.

- Hyperspectral imaging provides the resolution required to correct for atmospheric constituents within certain regions of the electromagnetic spectrum.[10]

1.2   Hyperspectral Imaging

Hyperspectral imaging continues to grow in popularity as an analytical tool. The high spectral resolution enhances the ability to discriminate between materials that are indistinguishable using other methods. The applications of this technology extend from the civilian sector through the military sector. Figures 1.4 and 1.5 demonstrate the ability to analyze mineral content in the soil at the Culprite Mine in Nevada. The images in Figure 1.4 provide a good spatial representation of the terrain but do not

4

provide the ability to distinguish similar minerals. However, the Tetracorder results, Figure 1.5, do distinguish kaolinite minerals as well as many others, separate kaolinite from alunite areas, and also indicate where both occur as mixtures by combining the spatial and spectral characteristics of the scene.

(a) Pseudo-true color

(b) Synthesized Landsat TM
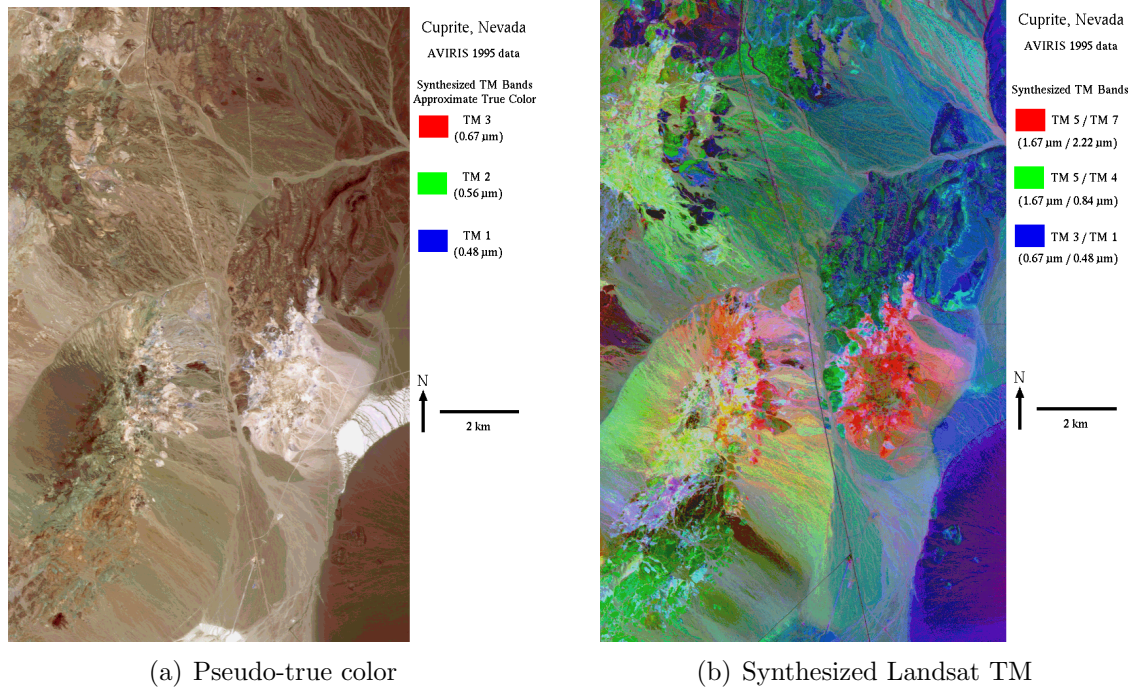
Figure 1.4: Images of Culprite Mine, Nevada constructed using AVIRIS data to simulate true color and Landsat TM images[11]

One of the major advantages of hyperspectral imaging is versatility. Hyperspectral imagers collect data over a nearly continuous spectrum with fine resolution. The combination of a nearly continuous spectrum and extremely fine resolution enables the sensor to provide useful information without considerable information about the target. Figure 1.6 is a representation of camouflage and vegetation reflectance in the visible and infrared (IR) regions of the electromagnetic spectrum. As expected, the reflectance is nearly the same for the camouflage and the vegetation in the visible regions. However, there are considerable differences, even between camouflage from different countries in the IR. A hyperspectral sensor operating in this region of the spectrum will detect these differences while use of a multispectral sensor requires band selection to look at particular regions within the spectrum. Appendix A lists many of the hyperspectral imagers in operation.
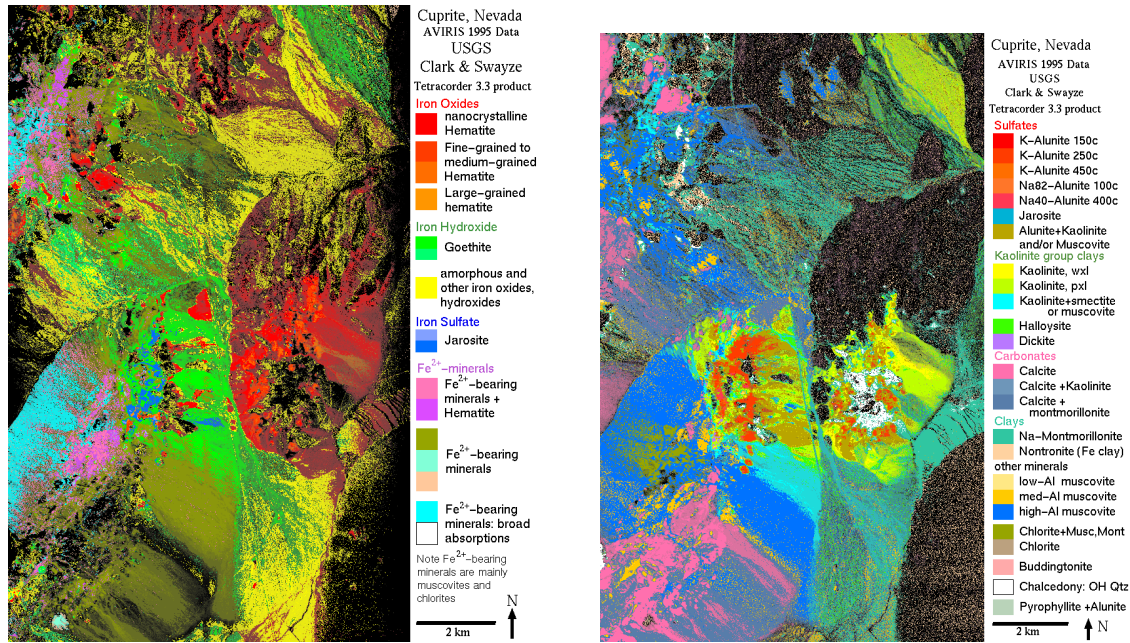
Figure 1.5: Tetracorder Mapping Results from AVIRIS Imaging Spectrometer Data Over Culprite Mine, Nevada[11]
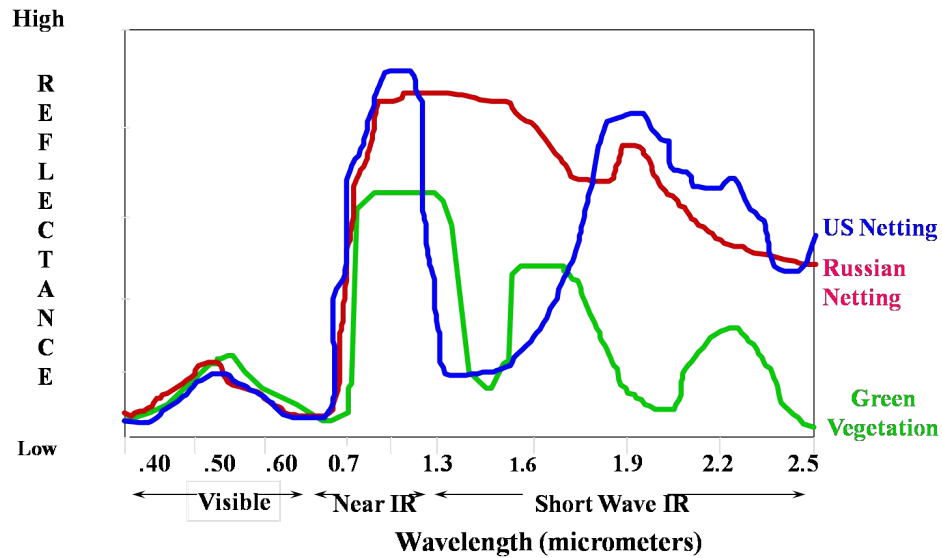
Figure 1.6: Reflectance of Vegetation and Camouflage

1.3 Chromotomography

Hyperspectral imaging does provide many advantages over panchromatic and multispectral imaging techniques. Although traditional grating hyperspectral imaging does allow the exploitation of the spectral resolution while accepting small tradeoffs with spa-

tial resolution, the current challenge is to capture fast transient temporal and spectral data with reasonable spatial resolution.

In the past, hyperspectral imaging was primarily limited to events characterized by spatial and spectral features that changed slowly (greater than one minute). The maturation of chromotomographic techniques makes it possible to examine fast transient events like the explosion shown in Figure 1.7. The majority of information is available for only the first 0.1 seconds while the entire event is over within about 1 second. This spectrum represents not only the initial explosion but the burning of by-products. These techniques use the same types of transforms used in medical tomography to reconstruct the spatial and spectral information convolved by the dispersive element.

(a) Visible EO Image
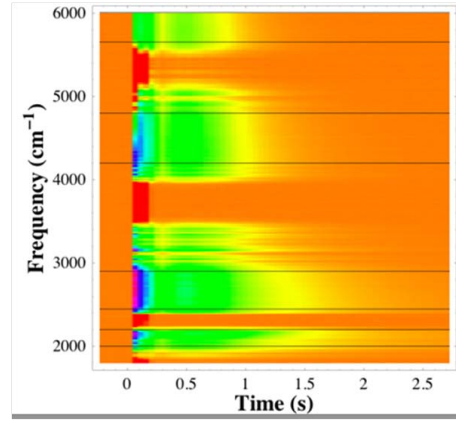
(b) 2D Spectral Plot
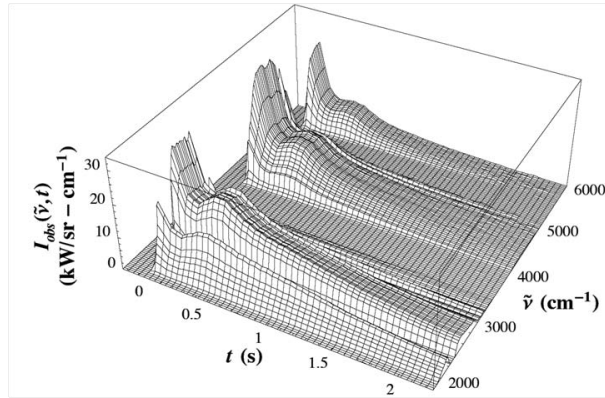
(c) 3D Spectral Plot with Intensity

Figure 1.7:   Spectral Analysis of Transient Explosion[4]

1.4 CTEx

CTEx is one application of chromotomography. While some of the phases may overlap, CTEx is segmented into three phases:

- Phase 1: Laboratory-based experiment. The Chromotomographic Hyperspectral Imaging System (CTHIS) is an initial proof-of-concept instrument. This instrument was used to determine the potential utility for this technique as well as development of an image reconstruction algorithm.

- Phase 2: Ground-based experiment, Figure 1.8. The ground instrument is actively used for data collection as a further proof-of-concept. The instrument will be used to collect data of progressively more temporally and spectrally transient events. The ultimate goal of this phase is to exploit fast changing combustion events outside the controlled laboratory environment. Successfully completing a data collection of this type will significantly reduce the risks associated with progression to space flight experiment.

Figure 1.8:   Ground-Based CTEx[4]

- Phase 3: Space flight experiment. This phase is the primary focus of this research. It is assumed that CTEx will be attached to the ISS on the Japanese Experiment

Module (JEM) External Facility (EF), Figure 1.9. This phase will validate the concept of implementing chromotomographic techniques from orbit and demonstrate that a chromotomographic payload provides the unique ability to collect data with high temporal resolution while balancing spatial and spectral resolution. These objectives will be accomplished by characterizing three different scenes[4]:

- Static hyperspectral scene: Demonstrate that CTEx can distinguish between a man-made object like a tank and surrounding vegetation.

- Large transient event: Demonstrate that CTEx can determine combustion constituents from a large-scale event like a forest fire.

- Point source transient event: Demonstrate that CTEx can determine combustion constituents from a point source such as a salt line characterization of a burner.
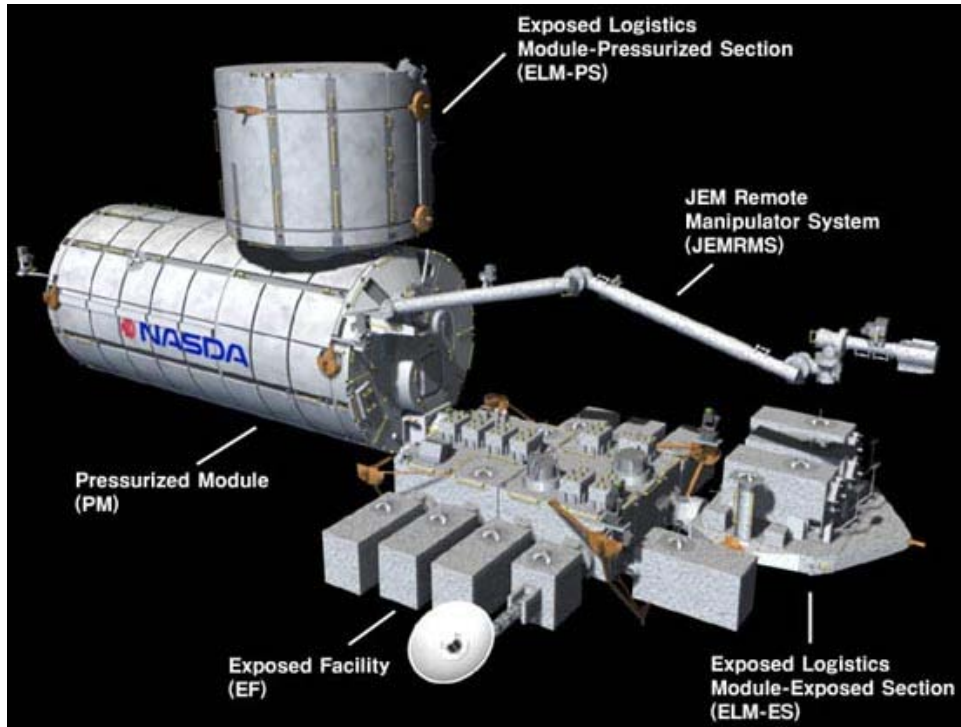
Figure 1.9:   JEM and EF (credit:JAXA)

Through all phases, the dispersive element used in CTEx is a rotating prism. The rotating prism design was chosen for several reasons:

- Less sensitivity to vibration and noise.

- Simple integration with standard imaging technologies.

- High optical throughput (no filters) lowers required signal to noise.

- Ability to perform non-imaging spectroscopy with the same data used to produce hypercubes.[12]

A general schematic of the CTEx instrument in use at AFIT is shown in Figure 1.10. L1 and L2 essentially serve as the telescope which collimates the light prior to the dispersive element. The rotating prism disperses the light according to wavelength. L3 is the focusing lenses which produces the image on the detector.
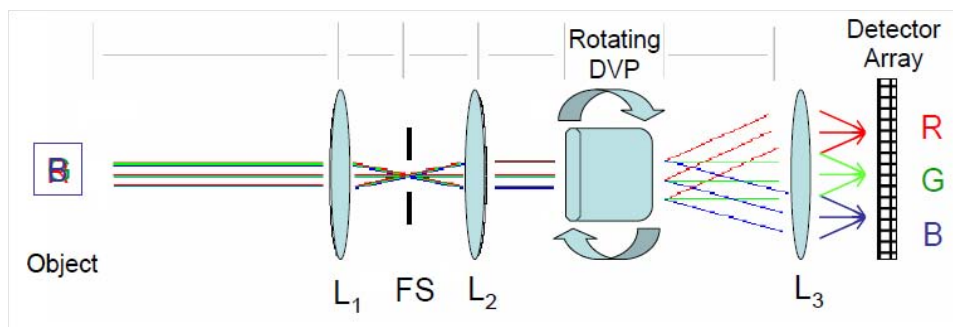
Figure 1.10:   Schematic of AFIT Chromotomographic Hyperspectral Imager[12]

1.5   Problem Statement

This research is a trade space analysis of the requirement to slew the space-flight CTEx to acquire and/or track a target. The trade space analysis will include three main topics:

1. Is there a requirement to slew CTEx? If so, how much does it need to slew and at what rate?

2. Is there a requirement to have on-board attitude determination?

3. What is the basic mission plan for CTEx?

Answering these three questions is fundamental to the development of the space-flight instrument. The telescope in currently in the design and construction phase and

can be immediately impacted to address some of these issues. Also, the ability to capture an image if a planned target is primarily influenced by the ability to precisely point the instrument. Without additional understanding of the pointing accuracy of the instrument and the attitude of the flight platform, the ISS, it is not possible to evaluate the mission profile for CTEx.

This thesis is organized into five chapters. The first chapter is an introduction to spectroscopy, hyperspectral imaging, chromotomography and CTEx to provide some basic background on the fundamental elements of this research. The second chapter is the detailed background and information found while conducting preliminary research. The third chapter is an description of the methodology used to analyze the attitude determination and slewing requirements for CTEx. The fourth chapter covers the results of the attitude determination and slewing analysis and develops the mission concept of operations for CTEx. The fifth chapter is a summary of conclusions and recommendations for future research.

II. Background

2.1 Literature Review

Prior to beginning work in an unfamiliar area it is wise to research previous and current efforts that might have an impact on one's own work. The literature review section of this chapter will cover some of the relevant existing sensors in operation today and the specifications of the ISS. The remaining sections will focus on slewing, attitude determination, and mission planning.

2.1.1 HICO-RAIDS. The Hyperspectral Imager for the Coastal Ocean (HICO) and the Remote Atmospheric and Ionospheric Detection System (RAIDS) Experimental Payload (HREP) is the most recent example of a space-borne hyperspectral sensor. The HREP was launched on 10 September 2009 and installed on the JEM-EF as shown in Figure 2.1 on 25 September 2009.

Of particular interest is the HICO payload shown in Figure 2.2. The HICO program has three main mission requirements:

- Build, launch, and operate the first space-borne Maritime Hyperspectral Imager (MHSI).

- Demonstrate the utility of a space-borne MHSI for both scientific and naval endeavors.

- Demonstrate innovative ways to develop and build an imager while reducing costs and schedule in support of the responsive space initiative.[13]

HICO uses a commercially-available all-reflective Offner grating Bradywine Optics model 3035 spectrometer and operates across 380 nm to 1000 nm spectral band. This range includes all of the water-penetrating wavelengths and a small portion of the near-IR to facilitate atmospheric corrections. The camera is a commercially-available QImaging Rolera-MGi science grade camera with a back-side illuminated CCD. The pointing mechanism is the commercially-available Newport Research model RV120PEV6 rotation stage. The rotation stage provides single-axis, cross-track pointing. Table 2.1 lists the specific performance requirements for the HICO payload.[14]
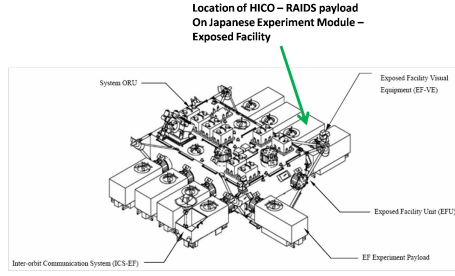
(a) Schematic Showing HREP at EFU#6. (credit: NRL)
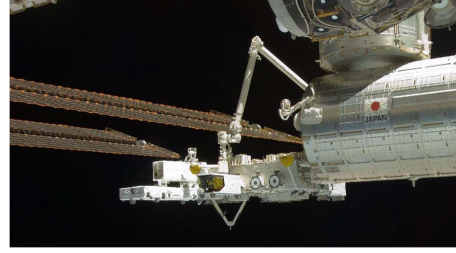
(b) Photo of HREP Installed on JEM-EF. (credit: NASA)
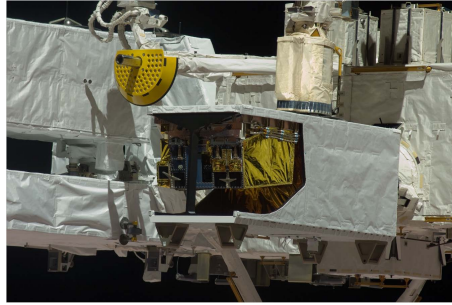
(c) Photo of HREP Installed on JEM-EF. (credit: NASA)

Figure 2.1:   Location of the HREP aboard the ISS.

Table 2.1:   HICO Performance Requirements

Parameter	Requirement
Ground Sample Distance at Nadir	100 m
Scene Size	50 km x 200 km
Spectral Range	380-1000 nm
Spectral Channel Width	5 nm
Number of Spectral Channels	124
Signal to Noise	>200:1
Cross-track Pointing	+45 to −30 deg
Jitter	<0.2 per integration period

(a) Photograph of the HICO payload.
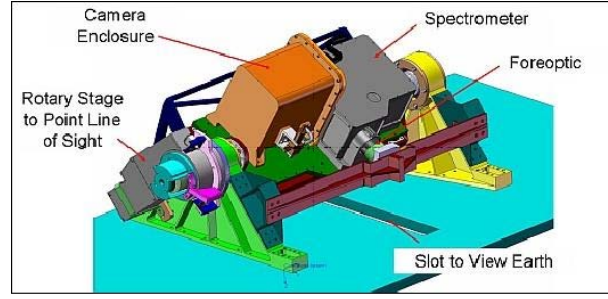
(b) CAD drawing of the HICO payload.

Figure 2.2:   HICO payload.

HICO is located at Exposed Facility Unit (EFU) 6, Figure 2.1. This unit is on the aft side of the JEM-EF and has an unobstructed Nadir view. Even with an unobstructed Nadir view, analysis of the instrument design indicated that a fixed sensor configuration did not meet the requirement to revisit any location accessible from the ISS orbit within 10 days.[15] Consequently, HICO incorporates cross-track slewing of +45 degrees to -30 degrees to increase access rates to target locations.[16] Also, initial analysis of the station's orbit and attitude accuracy indicated that the HREP required its own attitude determination system for RAIDS to determine attitude and for HICO to geolocate images.[16] The HREP has its own star tracker, a Terma HE-5AS Star Tracker, to meet this requirement.[17]

2.1.2   EO-1/Hyperion.   The Earth Observing 1 (EO-1) mission is part of the National Aeronautics and Space Administration's (NASA) New Millennium Program (NMP) and was launched from Vandenberg Air Force Base on November 21, 2000. The NMP was developed to validate new space-borne technologies and techniques for improved Earth observation. EO-1 carries three imaging payloads: the Advanced Land Imager (ALI), the Hyperion Imaging Spectrometer, and the Linear Eatlon Imaging Spectral Array (LEISA) Atmospheric Corrector (LAC). The ALI is a multispectral imager and the prototype for the new Landsat-7 Thematic Mapper. Hyperion is the first hyperspectral imager with high spatial resolution in Earth's orbit. The LAC is a wedge hyperspectral imager designed to determine atmospheric water vapor content.[18] Table 2.2 lists the major spatial and spectral characteristics of each imaging payload.

Table 2.2:   EO-1 Payload Characteristics.[18]

Parameter	Hyperion	ALI	LAC
Spectral Range	0.4-2.5μm	0.4-2.4μm	0.9-1.6μm
Spectral Resolution	10 nm	Variable	3-9 nm
Spectral Coverage	Continuous	Discrete	Continuous
Pan Band Resolution	N/A	10 m	N/A
Number of Spectral Channels	242	10	256
Spatial Resolution	30 m	30 m	250 m
Swath Width	7.7 km	37 km	185 km

Hyperion, shown in Figure 2.3, was built by TRW, Inc. while many of the sub-systems were contracted out: SSG Inc. designed and built the optical system; Boeing produced the short-wave IR (SWIR) focal plane array (FPA); Loral built the visible/near IR (VNIR) FPA; and Jet Propulsion Laboratory (JPL) fabricated the gratings.[19] The Hyperion instrument was designed to validate pushbroom performance and to provide high quality calibrated data for the evaluation of future hyperspectral imagers. It was placed in the same orbit as Landsat-7, trailing by about one minute, to accomplish this task. It was built and delivered for integration in less than a year and underwent precise calibration. Table 2.3 is a summary of pre-launch and on-orbit calibration results. These results achieved the goals of the Hyperion mission and solidified the utility of space-borne high spatial resolution hyperspectral imaging. The Hyperion instrument generates a standard image cube consisting of 660 frames of data (19.8 km long by 7.5 km wide) and collects the data in approximately three seconds.[20]

(a) End View   (b) Left View   (c) Right View
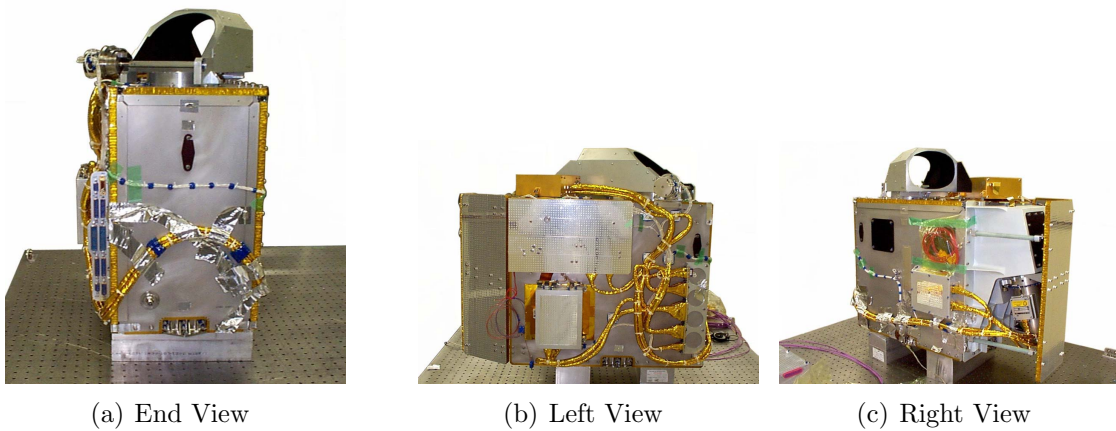
Figure 2.3:   Hyperion

Table 2.3: Hyperion pre-launch and on-orbit calibration results.[20] * values are similar to the pre-launch values within measurement error

Parameter	Pre-launch	On-orbit
GSD (m)	29.88	30.38
Swath Width (km)	7.5	7.75
Number of Spectral Channels	220	200
VNIR SNR (550-700nm)	144-161	140-190
SWIR SNR ($\approx$1225nm)	110	96
SWIR SNR ($\approx$2125nm)	40	38
VNIR Cross-track Spectral Error	2.8 nm at 655 nm	*
SWIR Cross-track Spectral Error	0.6 nm at 1700 nm	0.58
VNIR Spatial Co-registration	18% at Pix# 126	*
SWIR Spatial Co-registration	21% at Pix# 131	*
VNIR Bandwidth	10.19-10.21	*
SWIR Bandwidth	10.08-10.09	*

2.1.3 TACSAT-3/ARTEMIS. Tactical Satellite (TACSAT) is a joint Air Force Research Laboratory (AFRL) and Naval Research Laboratory (NRL) program designed to develop and demonstrate the capability to field inexpensive space systems in a time of crisis to augment or reconstitute existing systems or to provide additional capabilities.[21] TACSAT-3, shown in Figure 2.4, is the third in the series of satellites and hosts The Advanced Responsive Tactically-Effective Military Imaging Spectrometer (ARTEMIS) as its primary payload.[22] ARTEMIS was launched into a 425 *km* orbit in May 2009 and is currently the most responsive hyperspectral imager of Earth.[23]

The TACSAT-3 mission objectives include:[23]

- Demonstrate rapid response to a user-defined need for target detection and identification.

- Demonstrate rapid development of the space vehicle integrated payload and spacecraft bus using components and processes developed by the Operationally Responsive Space Modular Bus Program.

Figure 2.4: Artist's Rendering of TACSAT-3 with ARTEMIS Payload (credit:AFRL)[23]

- Demonstrate rapid deployment from alert status for launch to theater control (within seven days projected).

- Demonstrate responsive delivery of decision-quality information to operational and tactical commanders by enabling tactical tasking and data delivery.

- Deliver a fieldable capability within reasonable cost constraints.

ARTEMIS was designed with the goals of maximizing optical quality and simplicity while minimizing cost. To this end, ARTEMIS consists of a standard Ritchey-Chrétien telescope, a basic Offner grating imaging spectrometer, and a slightly modified high resolution Dalsa Piranha two line scan CCD camera.[22] Like CTEx, ARTEMIS only uses one FPA to collect data across the entire collection range. The imaging spectrometer samples at 5 nm intervals and maintains greater than 95% spatial and spectral uniformity. The high level of uniformity was essential to ensure the ability to produce high resolution images with geolocation of spatial and spectral data.[22]

One of the key capabilities that enables ARTEMIS to be a responsive asset is the ability to conduct on-board processing of data. The raw imagery data is processed on-board using spectral match indication and identification. The on-board processing capability enables anomaly detection and direct downlink to the warfighter.[24] ARTEMIS has demonstrated that it can collect, process and download a hyperspectral imagery product directly to a theater of operations during a single 10 minute pass.[23]

2.1.4 ISS Specifications.   The ISS is certainly an option that must be explored for remote sensing of Earth. The ISS's orbit at 51.6^o inclination is such that it flies over 85% of Earth's surface and 95% of the population. The station completes 16 orbits per day; each orbit crosses the equator 22.5^o to the West of the preceding orbit with a nodal regression of approximately 5° West per day. The solar beta angle varies between 0° and $+/-75^o$.[25]

Table 2.4 lists the attitude specifications for the ISS.

Table 2.4:   ISS Attitude Specifications[26]

Parameter	Characteristics
Range of Operational Attitude	Roll, Yaw: +/- 15 deg Pitch: +10 deg to -20 deg
Attitude Control Accuracy	+/- 5 deg per axis (compared to the commanded values) +/- 3.5 deg per axis (controlling to Torque Equilibrium Attitude)
Attitude Change Rate	+/- 0.02 deg/s per axis (except during microgravity experiments) +/- 0.002 deg/s per axis (during microgravity experiments)
Attitude Estimation Accuracy	0.5 deg per axis (3σ) 0.01 deg/s per axis (3σ)
Attitude Knowledge Accuracy	0.5 deg per axis (at NASA navigation base) 3.0 deg per axis (3σ) (at attached payloads)

2.2 Theory Behind CTEx

As mentioned in Chapter I, CTEx is an effort to exploit the capability that chromotomography has to balance spatial, spectral and temporal resolution as compared to other methods. Figure 2.5 depicts the trade space in each area. Although HSI does have the advantage of detecting more discrete spectral bands, CT balances all three areas and has the potential to provide exceptional temporal resolution. The high temporal resolution is the result of the high throughput attained by not using any filters. The high throughput enables the collection of low intensity emission spectra for classification and exploitation.

The method for obtaining spectral information is shown in Figure 2.6. The figure shows a mercury, Hg, pen lamp both pre-prism and post-prism. The pre-prism image shows the pen lamp as a point source with no ability to distinguish the different emission lines. In the post-prism view, the spread of the spectrum is clearly visible. The resulting line emission spectrum can then be compared to a reference library to determine the constituents. Figure 2.7 is the result of rotating the prism through a complete revolution. Each of the rings corresponds to a wavelength in the line spectrum in Figure 2.6.
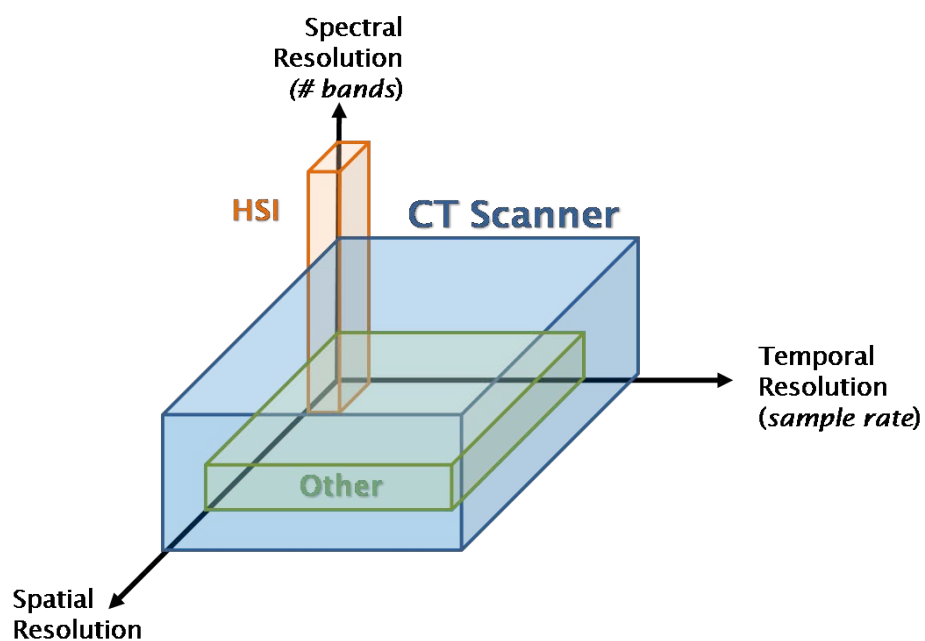
Figure 2.5:   Spatial, Spectral and Temporal Trade Space of Chromotomography.[4]
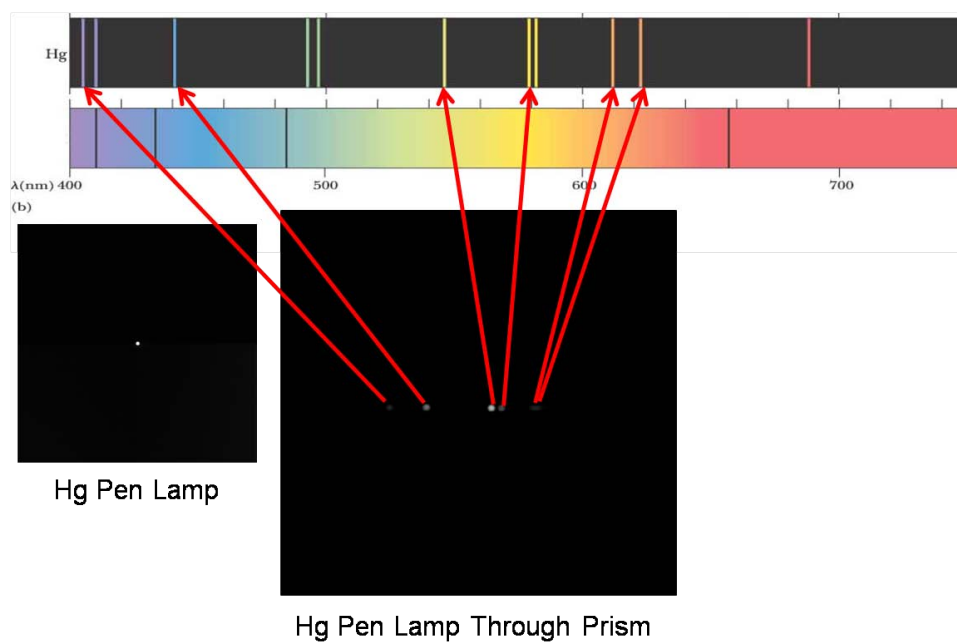
Figure 2.6:   Hg Pen Lamp Emission Spectrum as Seen Through CTEx[4]

Figure 2.7:   Hg Pen Lamp Emission: Output of CTEx Through 360° Rotation of the Prism[4]

The spatial information is obtained by implementation of a reconstruction algorithm. The algorithm takes the data shown in Figure 2.7 and creates a traditional data cube. Each point in each ring is aligned with the appropriate spatial pixel and then the individual wavelengths are stacked to create the data cube and spatial image. Essentially, only a small portion in the center of the FPA is used to collect spatial information at the undeviated wavelength. For the ground instrument, the undeviated wavelength is 550 nm.

The major trade is how much of the FPA is used for spatial information and how much is used to spread the spectrum for spectral resolution. Figure 2.8a shows a large area dedicated to spatial information. The disadvantage is that all of the bands overlap and spectral information is lost. Conversely, Figure 2.8b shows good spectral resolution, but a much smaller area of the FPA for spatial information at the undeviated wavelength; there is no overlap between wavelengths as the spectrum is spread across the FPA.
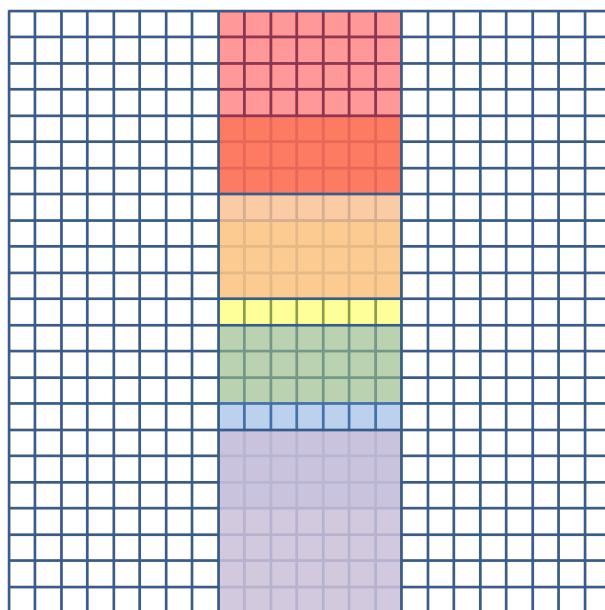
(a) High Spatial Resolution
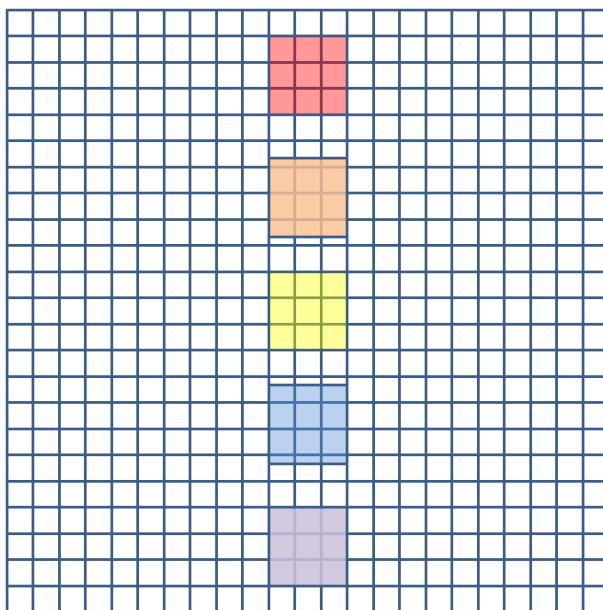
(b) High Spectral Resolution

Figure 2.8:   Spatial versus Spectral Resolution Trade Space

2.3 Slewing

There are two main configurations for sensors mounted on spacecraft. The first is a fixed sensor mounted at a specific azimuth and elevation. This option results in a fixed field of view (FOV) equal to the field of regard. The second is a gimbaled sensor. For this option, either the entire instrument or the FOV itself must be able to slew.[27] Cross-track and in-track slewing will be discussed throughout this thesis. Cross-track slewing is the displacement of the sensor or FOV normal to the orbital plane of the station. In-track slewing is the displacement of the sensor or FOV along the station's velocity vector.[28]

The first slewing option would require that the entire CTEx be mounted on some type of table and attached to one or more rotation stages. This is the type of technology used by HICO, and shown in Figure 2.2b, to achieve its cross-track slewing capability. The cross-track slewing is designed to increase target access rates and the field of regard; however, slewing in only the cross-track direction does not affect the collection time of the instrument. The collection time is affected by the in-track slewing only.

It is also possible to use a one or two axis slewing mirror to slew the FOV and increase the field of regard. One variation of this type of slewing is the scanning mirror utilized by Landsat Thematic Mapper (TM) shown in Figure 2.9. In this design, the scanning mirror moves left and right to scan across the entire field of regard to create an image. This concept can be modified to move the mirror to a fixed location and image across all pixels at once. This achieves the purpose of slewing in the cross-track direction. Using this mirror to slew in the in-track direction and then scanning at an angular rate equal to the satellite's angular rate serves as ground movement compensation to allow staring.

2.4 Attitude Determination

CTEx, like HICO, will be flown on-board the JEM-EF. As a secondary payload on the ISS, CTEx may require an on-board attitude determination system to ensure the necessary pointing accuracy. Fundamentally, CTEx must be able to know its attitude to precisely slew the imager and acquire a target.
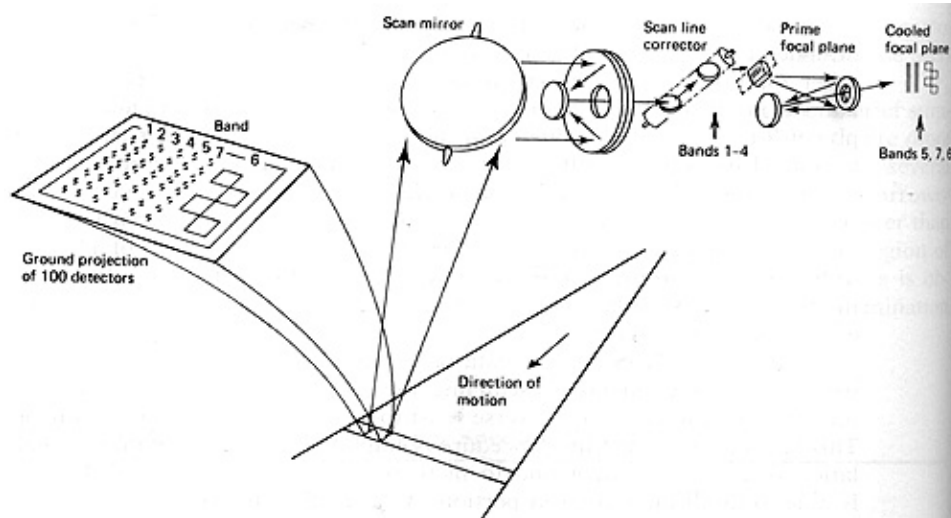
Figure 2.9:   Landsat TM Scanning Mirror Design.[11]

The goal of this analysis is to determine the accuracy of attitude knowledge required and to analyze what technologies can deliver the required performance. There are many different hardware solutions for traditional attitude determination:

- Magnetometers: These instruments measure the size and orientation of the surrounding magnetic field and their accuracy is limited by the precision of the geomagnetic model it uses. Magnetometers have achievable accuracies of 0.5 to 5.0 degrees (1,800 to 18,000 arcseconds) when used independently.[29]

- Radio Frequency Beacons: These instruments can only be used to determine pointing direction since only one reference is used. Accuracies of 1 arcminute (60 arcseconds) are achievable if a directional antenna is utilized.[30]

- Horizon Sensors: These instruments sense the limb of the Earth and can achieve accuracies of 0.5 to 1 degree (1,800 to 3,600 arcseconds).[28]

- Sun Sensors: These instruments only determine the pointing direction to the sun by looking for the brightest object and can achieve accuracies of 1 arcminute(60 arcseconds).[28]

- Solar Panels: Panels can be used to determine pointing direction by monitoring the currents from different solar panels and can achieve accuracies of 1 degree (3,600 arcseconds).[30]

24

- Global Positioning System (GPS): These instruments work by utilizing multiple GPS satellites and receivers and there corresponding pseudo-ranges to determine attitude. Depending on the baseline, the typical accuracies are approximately 6 arcminutes (360 arcseconds).[30]

- Star Trackers: These are the most accurate of the attitude determination systems can achieve accuracies of less than 1 arcsecond.[29]

Many of the technologies require the use of an inertial system to provide continuous attitude information. The technologies listed above are used to determine the absolute pointing direction and calibrate an inertial system. The inertial system then measures the changes in attitude between calibrations. However, second generation star trackers or imagers do not require the additional inertial system. These star trackers contain a powerful microcomputer equipped with mathematical models of the spacecraft's motion. The models are accurate enough to propagate its attitude.[30] Section 3.3.1 describes in detail the attitude knowledge capabilities of the ISS. Generally speaking, the ISS has the ability to transmit attitude information within 0.3 degrees (1080 arcseconds) to attached payloads. There exists the need to determine the attitude of CTEx to within 90 arcseconds, described in Section 4.2.

2.5 Mission Planing

Mission plans are the basis for how a satellite or secondary payload operates. Mission plans establish the procedures for operations and provide detail as to who is responsible for what task and how and when each task is accomplished.[31]

There are several key factors that impact a mission plan:

- Launch to Installation Timeline. This schedule will be determined by the agency that owns the launch vehicle. HREP flew on the H-II Transfer Vehicle (HTV) and followed the timeline provided by JAXA shown in Figure 2.10. The HERP timeline required 15 days from launch until the payload was operational.

- Command List Submission. CTEx will have very specific requirements and timelines that must be followed to meet NASA's planning scheme. In general, a list

of commands that the instrument will execute is sent to NASA for approval three weeks prior to execution. There is a review of scheduled commands one week prior to execution. Finally, there is a final confirmation of commands three days prior to execution. The structured procedure means that there is very little chance that payload commands can change on short notice. The one to three week lead time on commands will likely require that CTEx be able to determine its attitude and position and calculate all slewing and collection times based off of target location.

- Data Rates and Transmission Times. There are various data transmission rates on-board the ISS. The payloads on the ISS must share bandwidth and transmission time. Figures 2.11 and 2.12 lists the different types of data communications available on the ISS as well as actual data rates for several facilities and experiments.

- Autonomy. The autonomy built into satellites and payloads varies dramatically. On the low end, each command that a payload executes must be uploaded from a ground station based on the input of an operator. On the high end, a payload receives minimal inputs from an operator and generates its own commands using complex algorithms on-board.

Of specific interest is the level of autonomy demonstrated by satellites today. EO-1 is an excellent example of a satellite with multiple payloads that used a low level of autonomy in the past, but validated autonomy tools during flight. The Autonomous Sciencecraft Experiment (ASE) is a set of integrated technologies that enable autonomous science data collection, processing, and downlinking. It includes the Continuous Activity Scheduling Planning Execution and Replanning (CASPER) software and the Spacecraft Command Language (SCL) package.[31]

The ASE allows the spacecraft to use a set of priorities and goals uploaded from a ground station to plan collection opportunities, collect an image, analyze the image for changes and quality, and discard or downlink the image based on results.

Table 1: HTV Mission Timeline (JAXA, Aug. 27, 2009)

Flight Day	Tasks
1	Launch/Insertion, post-insertion auto sequence (the HTV subsystem activations, attitude control, self-check, TDRS communications establishment, initiation of communication with the HTV Mission Control Room (MCR), TKSC, far field rendezvous flight maneuver
2	Far field rendezvous flight maneuver
3	Far field rendezvous flight demonstrations: Collision Avoidance Maneuver (CAM), passive abort and attitude control, correction from large attitude deviation, Free Drift
4–6	Far field rendezvous flight maneuver
7	IMMT review on the HTV demonstration operations data ; Arrival at the HTV PROX range
8	ISS proximity operations, final approach, capture by station's robotic arm, berthing to the ISS critical vestibule outfitting, activation of the HTV subsystems
9	Vestibule outfitting, crew ingress, cargo transfer (from HTV to ISS)
10–11	Cargo transfer from HTV to ISS
12	Temporary installation of the Exposed Pallet (EP) to Kibo Exposed Facility (EF)
13–14	Transfer and installation of HREP and SMILES to the Exposed Facility (EF)
15	Removal of the EP from the EF and reinstallation of the EP onto the HTV (robotic operation), transfer of waste and used materials from the ISS to the HTV (Inter-vehicular activity)

Figure 2.10:   HREP Launch to Installation Timeline(Photo Credit: top image: JAXA, bottom image: NASA)[32]

Actual Data Rates: First 18 months of Columbus operation

- Data communication types
  - Payload 1553B interface Bus: low data rate and housekeeping telemetry (all payloads must use this interface) via analogue, discrete and serial connections to the payload control unit
  - Medium data rate: Standard Ethernet LAN, limited to 10Mb/s (currently restricted 3Mbps). Future evolution may permit data rates up 100Mb/s
  - High data rate: Fibre optic line Up to 32Mb/s/channel to be expanded to 120Mb/s/channel
- Examples of actual data rates
  - ESA EDR Facility: ~2Mb/s near continuously for an operating run of 120 days total duration (During LOS data dumped to HCOR)
  - ESA EVC experiment externally attached to CEPF: ~2Mb/s for 6-8h once per week, supplemented with ~2Mb/s for 1h each day.
  - ESA FSL facility: 8Mb/s for 6-8h period once per week
  - JAXA MAXI Instrument (on Kibo-EF): 0.6Mb/s continuous
  - JAXA SMILES Instrument (on Kibo-EF): 0.2Mb/s continuous

Figure 2.11:   ISS Data Rates.[25]

JEM-EF Resources	
Mass capacity	550 kg (1,150 lb) at standard site 2,250 kg (5,550 lb) at large site
Volume	1.5 m³
Power	3-6 kW, 113-126 VDC
Thermal	3-6 kW cooling
Low-rate data	1 Mbps (MIL-STD-1553)
High-rate data	43 Mbps (shared)

Figure 2.12:   JEM Data Rates.[33]

2.6   Summary

While many of the operating parameters of CTEx are demonstrated to some extent by existing technologies, CTEx is an instrument that provides a new capability in the hyperspectral imagery community:

- CTEx provides a unique capability to image not only slowly-changing events but fast-transient events as well. Like HICO, CTEx is planned to be flown on-board the JEM-EF. HICO has a large FOV relative to that of CTEx; yet HICO required the ability to slew to meet revisit requirements. Specifically, HICO was mounted on a rotation stage with a slewing range of 75 degrees.

- CTEx is designed to be sensitive to a smaller spectral band than Hyperion; however, CTEx does provide more temporal resolution. Also, Hyperion collects and stores about three seconds of data. CTEx is required to obtain 10 seconds of data to ensure the collection of very transient events. The increased data storage and transmission requirements will necessitate improving the type of technology that Hyperion is using.

- EO-1 utilizes software capable of providing virtually any amount of autonomy required. The payloads on-board EO-1 can be controlled with detailed commands

28

uploaded from a ground site or autonomously controlled by on-board processing based on minimal input from the operators. This technology may provide the capabilities that CTEx requires to image point sources even with a small FOV.

III. Methodology

This chapter covers the relevant equations and methodology for analysis of the slewing and attitude determination requirements for CTEx. The initial trade space was developed using actual two line element sets (TLEs) for the ISS obtained on CelesTrak at celestrak.com.

3.1 Slewing

3.1.1 In-Track Slewing Requirement. The FOV, ground track velocity, and angular rate of the sensor can be calculated using the sensor half angle and the altitude of the ISS.

The Nadir circular FOV, shown in Figure 3.1, can be calculated using Equation 3.1 where R is the ground projection radius of the detector array, h is the altitude, and θ is the angular diameter of the field of view.[28]

$$FOV_{Nadir} = \pi R^2 = \pi \left(h \tan \left(\frac{\theta}{2} \right) \right)^2 \tag{3.1}$$

Equation 3.1 must be modified slightly when calculating the FOV of a gimbaled sensor, shown in Figure 3.2. The calculation must take into account the angle that the sensor moves away from Nadir. The movement off-Nadir requires that the FOV be corrected as the projection onto the Earth. The off-Nadir circular FOV of a slewing sensor is determined using Equation 3.2 where γ is the angle off-Nadir.[28]

$$FOV_{offNadir} = \pi R^2 = \pi \left(\frac{h}{\cos \gamma} \tan \left(\frac{\theta}{2} \right) \right)^2 \tag{3.2}$$

The circular velocity, V_c, and orbit period, T, of the ISS can be determined using Equations 3.3 and 3.4 respectively where μ is the Earth's gravitational constant, 398,600.5 km^3/s^2, and r is the orbit's radius ($R_E + h$).[28]

$$V_c = \sqrt{\frac{\mu}{r}} \tag{3.3}$$
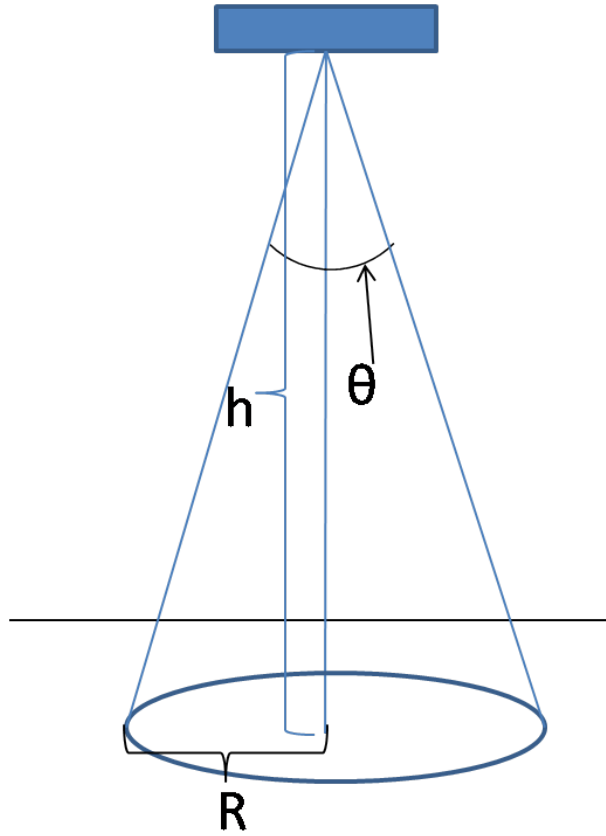
Figure 3.1:   Nadir FOV
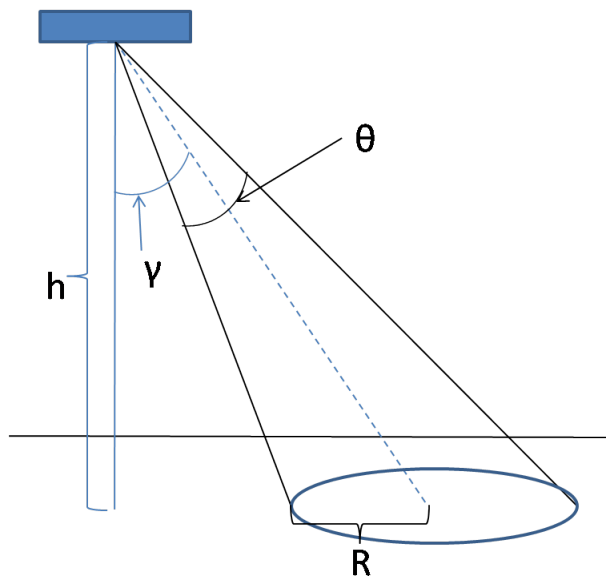
Figure 3.2:   Off Nadir FOV

$$T = 2\pi \sqrt{\frac{r^3}{\mu}} \tag{3.4}$$

Using the orbit period, T, and the radius of the Earth, $R_E = 6378.135\ km$, Equation 3.5 is used to determine the velocity of the subsatellite point, V_{gt}, the point on the Earth's surface corresponding to the projection of the satellite onto the Earth.[28] The time it takes that subsatellite point to travel the circumference of the Earth is equal to the period of the satellite.

$$V_{gt} = \frac{2\pi R_E}{T} \tag{3.5}$$

Again focusing on the Nadir case, it is possible to determine how long a target will be in view if CTEx does not slew using Equation 3.6. Figure 3.3 shows how the target, in this case Dayton, OH, moves through the FOV during an access period. The in-view time, $t_{Nadirview}$, for Dayton is equal to the time that Dayton is within the cone representing the FOV of the instrument. The maximum in-view time will occur when the target passes through the center of the FOV.

$$t_{Nadirview} = \frac{2R}{V_{gt}} \tag{3.6}$$

Finally, the instrument must be able to slew in-track at a rate equal to the angular rate of the ISS with respect to a ground station, ω, which is calculated using Equation 3.7 where h is the station's altitude and V_c is the orbital velocity.

$$\omega = \frac{V_c}{h} \tag{3.7}$$

3.1.2   Cross-Track Slewing Requirement.   The need to slew in the cross-track direction is driven by the frequency of accessing a target. The analysis was conducted using Satellite Tool Kit (STK) by Advanced Graphics Incorporated. The CTEx instrument with no slewing capability was modeled as a fixed simple conic sensor with a half angle of 0.05 degrees.[34] The slewing sensor options were modeled as fixed rectangular
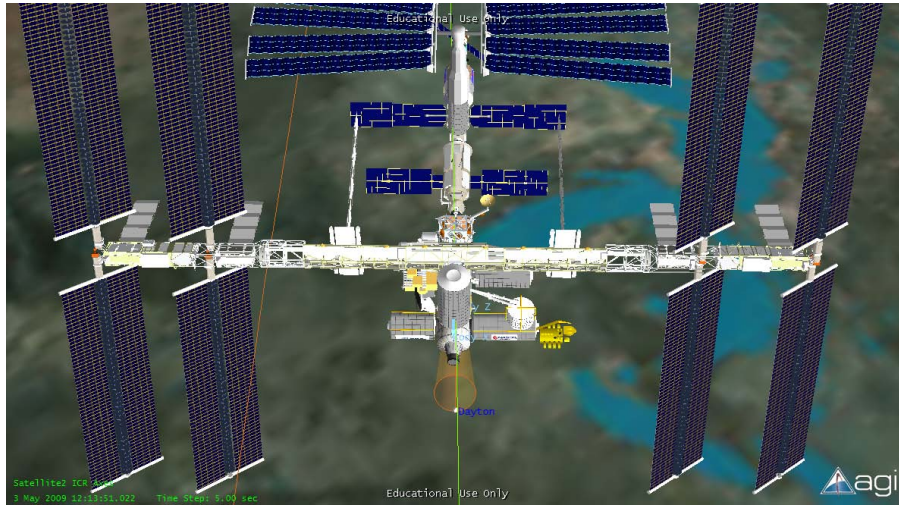
(a) Enter the FOV
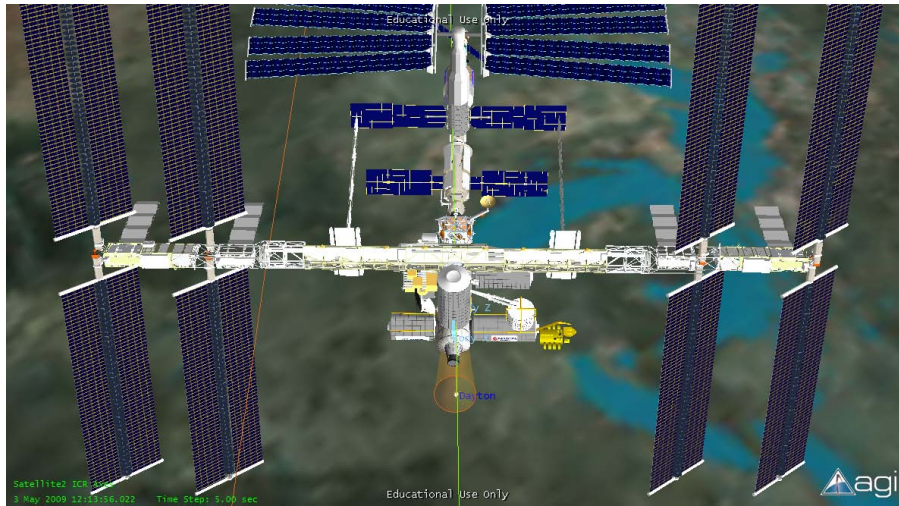
(b) Middle of FOV (Nadir)
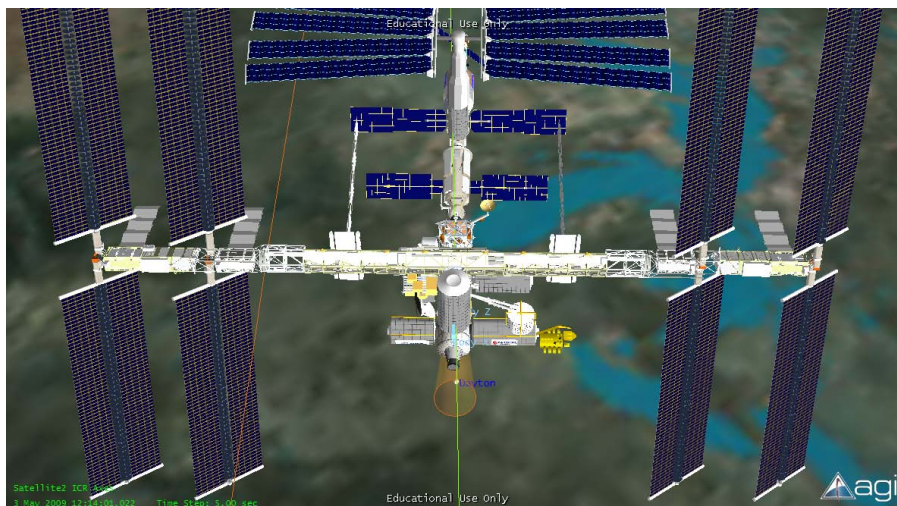
(c) Exit of FOV

Figure 3.3:   In-View Time for a Fixed Sensor

sensors with 8 degrees of in-track, x-axis, ground movement compensation and varying ranges of cross-track, y-axis, slewing capability.

The two targets of interest for this study were Dayton, Ohio and Mount Washington, New Hampshire. Wright-Patterson Air Force Base and the Air Force Institute of Technology are both located in Dayton and provide convenient locations for test sites and data analysis. Mount Washington has been used to conduct salt line burner tests in the past and provides an established facility for the CTEx demonstration. The seven calibration facilities of interest were the six pseudo-invariant sites and Frenchman Flat. These sites were selected from the long list of calibration sites because they are well established United States Geological Survey (USGS) sites. The pseudo-invariant sites are large uniform sites and Frenchman Flat is a monitored site with online calibration data updated every five minutes.[35] All of the sites are depicted in Figure 3.4. Figure 3.5 shows that the station's orbit does cover all nine of these sites and that they can be observed given enough slewing capability.

3.2   STK Model Development

There are several methods of modeling the two-axis slewing capability of the sensor; however, the choice was made to model it as a rectangular sensor. This technique models the sensor's field of regard vice the field of view and is the most efficient means of determining the slewing requirements from target access. Figure 3.6 depicts the 0, 8, 13, 18, and 23 degrees of cross-track slewing capability and their respective fields of regard. 0° was chosen to evaluate the case with no slewing; 8° was chosen to evaluate the slewing option equal to the dwell mirror slewing capability; 13°, 18° and 23° were chosen to evaluate slewing options that require the entire instrument to slew on a rotation table using a rotation stage.

The sensors were added to the model of the ISS and moved to a fixed location on the JEM-EF. The sensors were modeled as fixed rectangular sensors and the horizontal half angle was sent to 8 degrees for all sensors and the vertical half angle was sent to 0.05, 8, 13, 18, and 23 degrees for the five different cross-track slewing capabilities. The sensors were attached to the JEM-EF by establishing the attachment point using a Cartesian
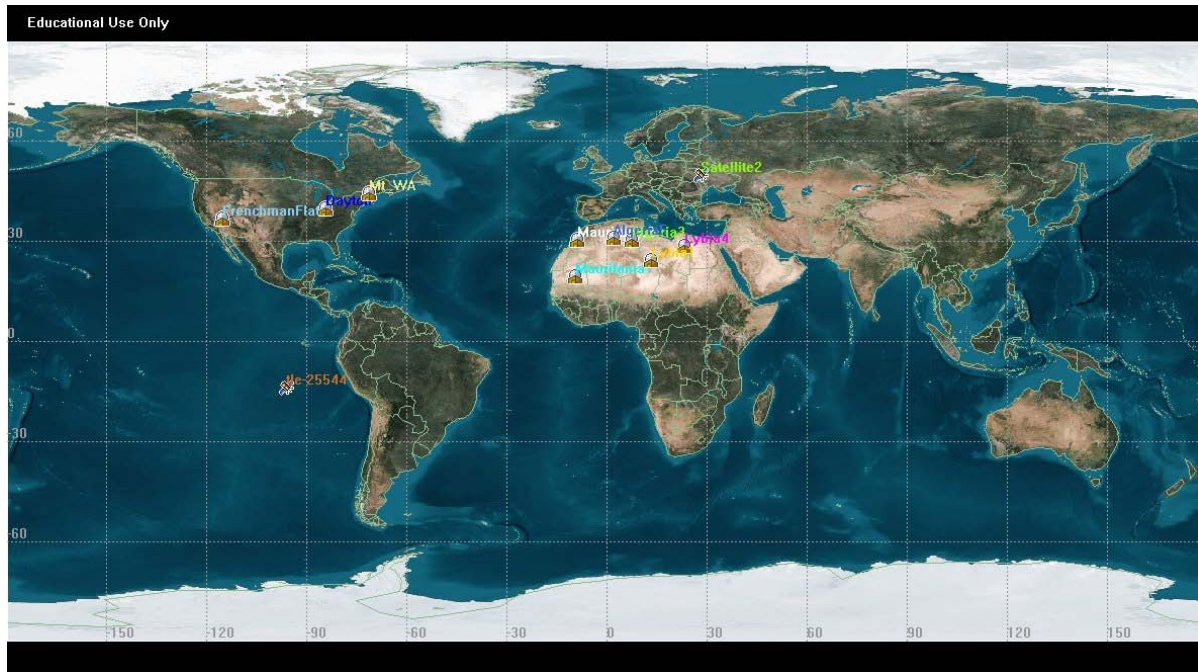
Figure 3.4:   Target and Calibration Site Locations
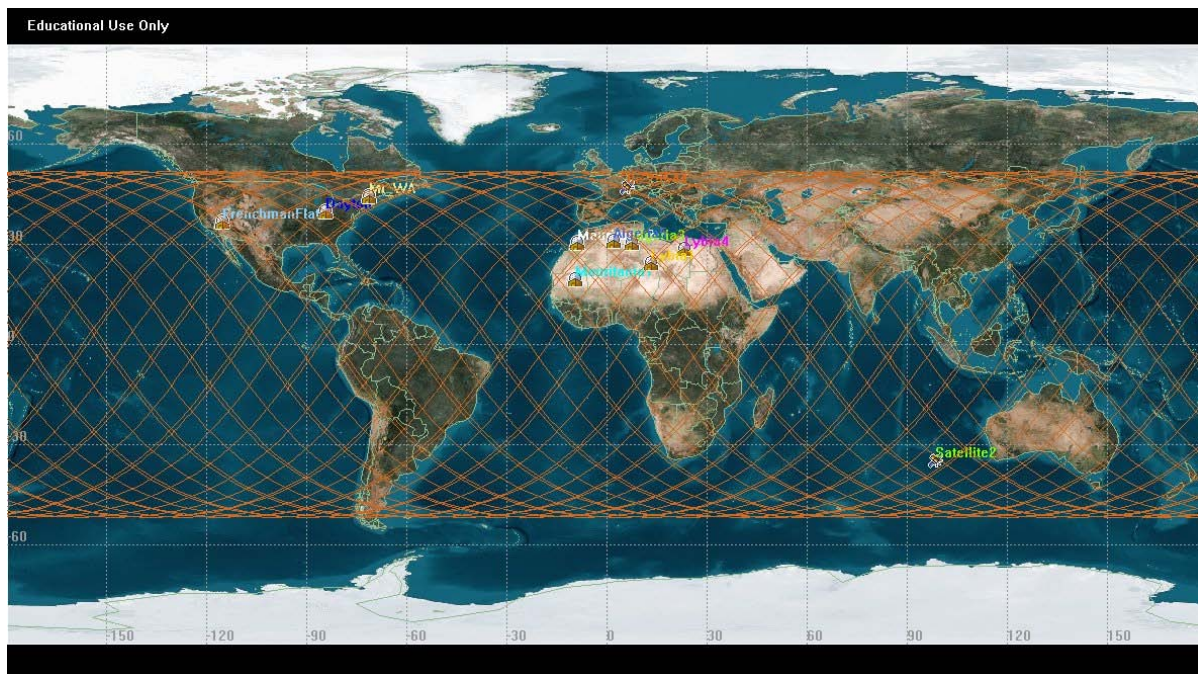
Figure 3.5:   Nine Target Locations Overlayed with the Ground Track of the ISS.
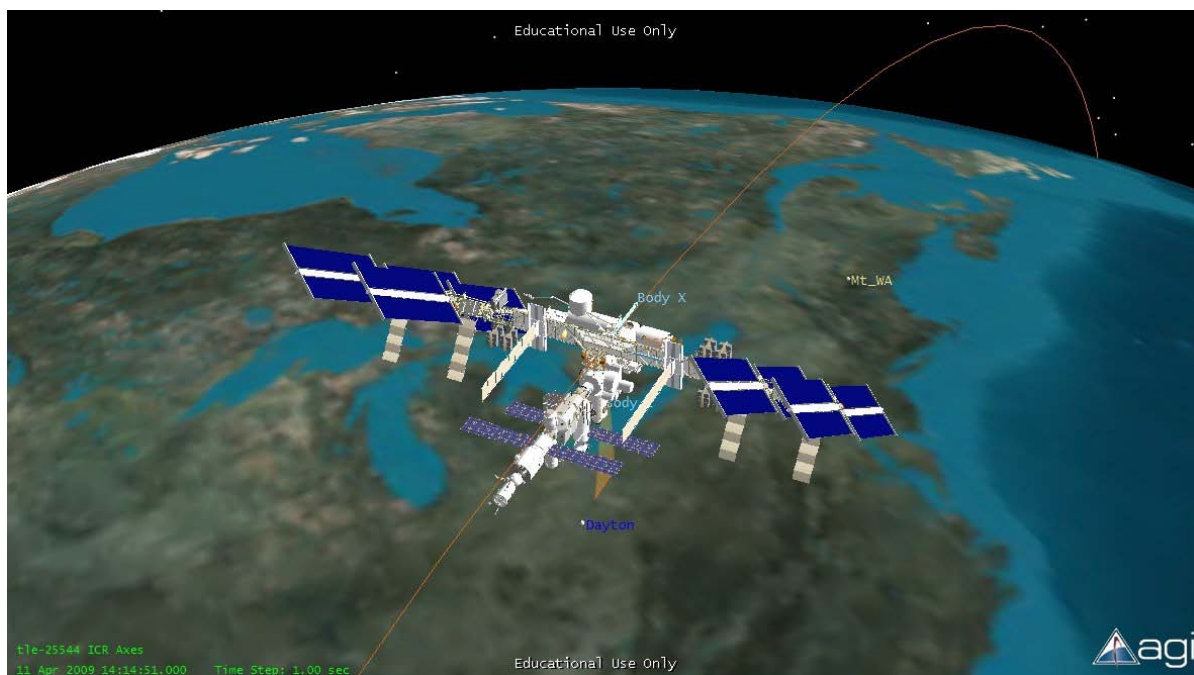
(a) 0 degrees of cross-track slewing

(b) Each box represents 8, 13, 18 and 23 degrees of cross-track slewing

Figure 3.6:   CTEx Field of Regard With Five Slewing Capabilities

offset; the X, Y, and Z values were 0.0122 km, -0.015 km, and 0.0073 km respectively. These values are the offset from the origin of the model in STK to the JEM-EF model in STK.

The targets and facilities were added to the scenario as facilities within STK. The location of each target and calibration site was established using the latitude and longitude values listed in Table 3.1. Each of the calibrations sites will only be utilized during daylight. This constraint was established by setting the lighting constraint to direct sunlight for each calibration site.

Access reports were then generated for each of the nine target and calibration sites for all five sensor configurations. All reports covered the entire scenario time. These reports, discussed in Chapter IV, indicate the number of times in the six month period that each of the sites was in-view given the established lighting constraints and sensor parameters.

3.3   Attitude Determination

The accuracy of the knowledge of the attitude of CTEx in flight is paramount to the ability to point the instrument at any given target. All planned experimental targets, discussed in Section 1.4, can be considered point targets except for the slow-changing combustion event which is currently planned to be a forest fire or other large-scale event. The large-scale combustion event will require considerably less pointing precision purely due to the area on the ground covered by the event.

Table 3.1:   Target and Calibration Site Locations

Site Name	Site Type	Latitude (deg)	Longitude (deg)
Dayton, OH	Target	39.7791	-84.1974
Mt. Washington, NH	Target	44.2703	-71.3033
Algeria 3	Calibration	30.32	7.66
Algeria 5	Calibration	31.02	2.23
Libya 1	Calibration	24.42	13.35
Libya 4	Calibration	28.55	23.39
Mauritania 1	Calibration	19.40	-9.30
Mauritania 2	Calibration	20.85	-8.78

3.3.1 ISS Position and Attitude Accuracy.   NASA provides both long-term and short-term ephemeris data for the ISS. A weekly analysis is conducted and ephemeris predictions are produced for 18 months and four weeks. The four week predictions are the most accurate while the 18 months predictions serve as planning tools for re-boost and attitude change procedures.[16]

The short-term predictions have been shown to produce values for position within $1\ km$ in each axis and velocity within $0.9\ m/s$. On-board, the ISS utilizes four GPS receivers at different locations to measure position and velocity. These measured values are better than $75\ m$ in each axis for position and better than $0.2\ m/s$ for velocity. The station also uses differential GPS to determine attitude to within $+/-$ 3 degrees. Some of the other facilities on the ISS are capable of determining attitude and sharing it with other payloads. Specifically, the JAXA Kibo module is capable of providing attitude within 0.3 degrees and sharing that information with other Kibo-EF payloads.[36]

3.3.2 Required Attitude Knowledge of CTEx.   The error in attitude knowledge required to potentially see a target is calculated by determining the maximum error that yields a pointing accuracy equal to half the radius of the FOV. The highest degree of pointing accuracy is required when the FOV is smallest, or when the sensor is Nadir pointing. The primary component of the pointing error is the accuracy of the attitude of CTEx. The assumption is that the pointing accuracy be within $\frac{1}{2}R$ to ensure that the target is within the center of the FOV. Figure 3.7 shows how attitude effects the boresight of the sensor. If the pointing accuracy, a combination of several factors including attitude knowledge, of the sensor is worse than the twice the radius of the FOV, then the target will potentially fall outside the FOV, Figure 3.7a. Improving the pointing accuracy to equal the radius of the FOV results in the target falling somewhere within the limits of the FOV, Figure 3.7b. Figure 3.7c represents the potential target locations within the FOV when the pointing accuracy is improved to one half of the FOV. Limiting the pointing accuracy to half the FOV ensures that the target does not fall on the edge of the FOV and decreases the chances of missing a collection.

(a) $h\Delta\theta > 2R$

(b) $h\Delta\theta = R$

(c) $h\Delta\theta = \frac{1}{2}R$
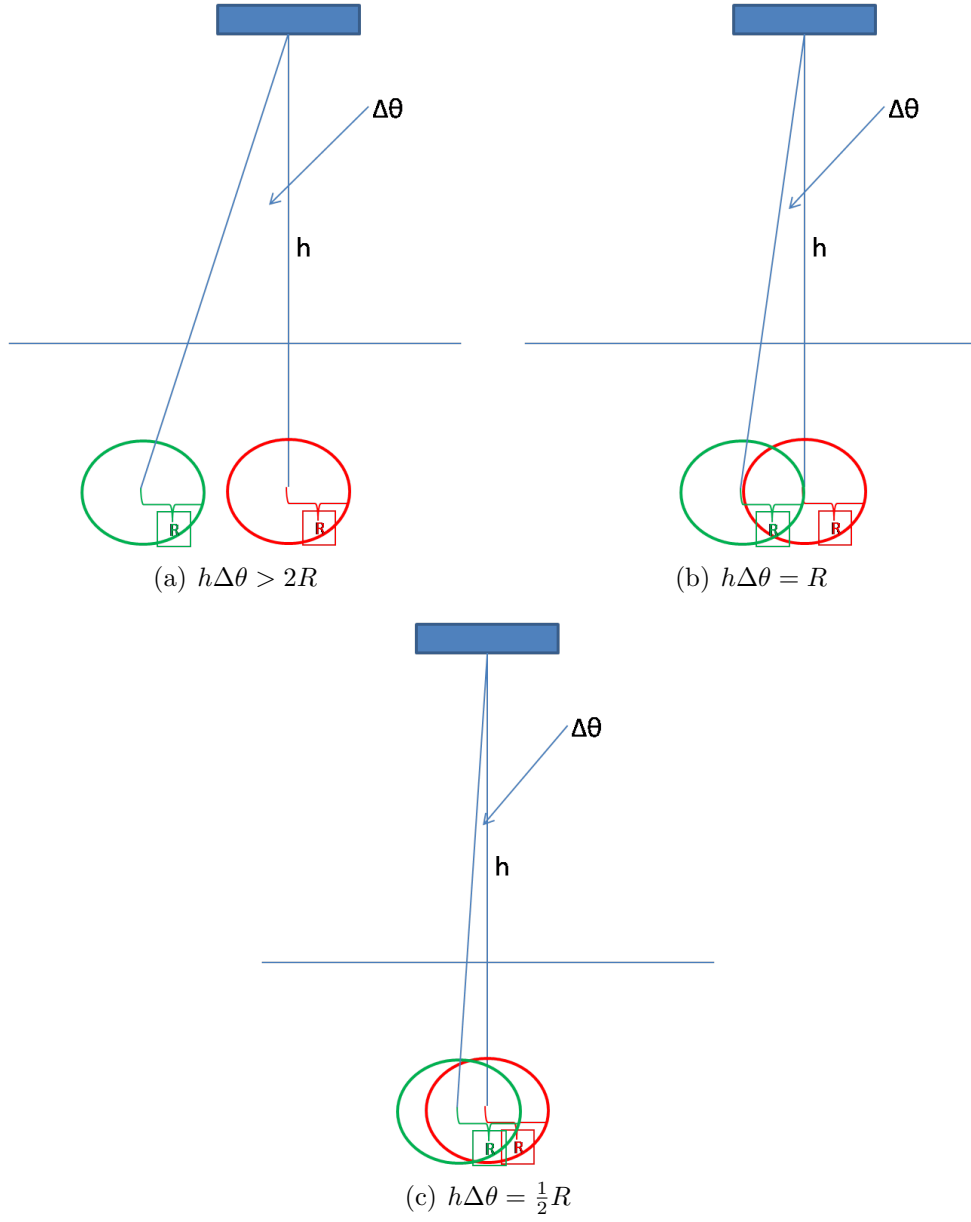
Figure 3.7:　　Effects of Pointing Accuracy

Using Equation 3.1 we can develop the expression for R shown in Equation 3.8 where θ is the angle off boresight (Nadir in this case) and h is the altitude of the imager (450 km). The equation is rearranged to solve for θ, Equation 3.9.

$$R = h \tan(\theta) \tag{3.8}$$

$$\theta = \arctan\left(\frac{R}{h}\right) \tag{3.9}$$

3.4 Summary

This chapter describes the fundamental equations necessary to evaluate the pointing requirements of CTEx. The equations and models will be used in Chapter IV to determine the slewing and attitude determination requirements for CTEx at the current altitude of 350 km and the planned altitude of 450 km. The resultant requirements will be incorporated into STK to develop the initial concept of operations for CTEx from launch to operation.

IV. Results and Analysis

This chapter covers the required slewing and attitude determination capabilities for CTEx. The analysis was conducted using STK and actual TLEs covering a period of six months from from 10 April 2009 to 15 October 2009. The invariant altitude of the station is used throughout this analysis. The invariant altitude (IA) is the mean altitude of each orbit. The IA removes the small differences in altitude caused by the slight eccentricity of the orbit and the shape of the Earth. During this time period, the IA of the ISS ranged from 346 km to 352 km. These results were then used to develop the mission plan for CTEx from launch to experimental data collection and downlink.

4.1 Slewing

4.1.1 In-Track Slewing Requirement. The CTEx telescope is currently in the acquisition phase and the decision has been made to slew the instrument in-track using a slow steering mirror with a range of +/- 8 degrees. This section will determine if this range meets the required collection time of 10 seconds. This analysis uses an altitude of 350 km and assumes the orbit to be circular. Although the station's orbit is not exactly circular, it is a reasonable assumption since its eccentricity is 0.0009, as reported in the TLEs.

The Nadir FOV and FOV diameter, $2R$, are calculated using Equations 4.1 and 4.2 where R is the ground projection radius of the detector array, h is the altitude, and θ is the angular diameter of the field of view. CTEx has a half angle, $\frac{\theta}{2}$, of 0.05 degrees.

$$FOV_{Nadir} = \pi R^2 = \pi \left(350 \tan\left(0.05^o\right)\right)^2 = 0.293 km^2 \tag{4.1}$$

$$2R = 2\left(350 \tan\left(0.05^o\right)\right)^2 = 610.9m \tag{4.2}$$

The off-Nadir circular FOV and FOV diameter, $2R$, of CTEx at maximum deflection is determined using Equations 4.3 and 4.4 where γ is the angle off-Nadir, 8° of dwell mirror movement in the in-track direction.

$$FOV_{offNadir} = \pi R^2 = \pi \left(\frac{350}{\cos 8^o} \tan (0.05^o) \right)^2 = 0.298 km^2 \tag{4.3}$$

$$2R = 2 \left(\frac{350}{\cos 8^o} \tan (0.05^o) \right)^2 = 616.9m \tag{4.4}$$

The circular velocity, V_c, and orbit period, T, of the ISS were determined using Equations 3.3 and 3.4.

$$V_c = \sqrt{\frac{398,600.5 km^3/s^2}{6378.135km + 350km}} = 7.697 km/s \tag{4.5}$$

$$T = 2\pi \sqrt{\frac{(6378.135km + 350km)^3}{398,600.5 km^3/s^2}} = 91.538 min \tag{4.6}$$

The velocity of the ISS's subsatellite point was calculated using Equation 3.5.

$$V_{gt} = \frac{2\pi 6378.135km}{5492.28s} = 7.296 km/s \tag{4.7}$$

Finally, the time that a target is in view if CTEx does not slew was calculated using Equation 3.6. This collection time clearly does not meet the 10 second requirement.

$$t_{nadirview} = \frac{610.9m}{7296m/s} = 0.0837s \tag{4.8}$$

With a fixed telescope design, increasing the in-view time requires that CTEx be able to slew. The required slewing rate for CTEx was calculated using Equation 3.7.

Meeting the 10 second collection time requires approximately +/- 6 degrees in-track slewing capability as shown in Equation 4.9.

$$\omega = \frac{7.697 km/s}{350 km} = 0.02199 rad/s = 1.26 deg/s \tag{4.9}$$

STK was used to determine the in-view time for both Dayton and Mt. Washington using the dwell mirror in-track slewing range, +/- 8 degrees. This range enables CTEx to track a target and collect data for approximately 14 seconds at the current altitude of 350 km. The progression of calculations followed above was repeated for the planned station altitude of 450 km, Table 4.1. At 450 km, CTEx will be able to view a target and collect data for approximately 17 seconds. The next section will focus on the cross-track slewing requirement.

4.1.2 Cross-Track Slewing.   The cross-track slewing requirement was analyzed through the production of access reports in STK. Table 4.2 lists the number of access to each target site (no lighting constraints) and each calibration site (direct sunlight) for each sensor configuration at both the current altitude of 350 km and the planned altitude of 450 km. In several cases, the number of calibration site accesses for a given sensor actually decreases when the altitude of the station is increased. This seems counterintuitive; however, the decrease is site access is due to the lighting constraint. There are actually more accesses, but they occur during periods when the site is not illuminated by direct sunlight.

The fact that there were zero accesses to any of the sites over the six month period without slewing indicates that CTEx must slew in the cross-track direction. The slewing range selection is a matter of satisfying mission requirements and system design. CTEx is a proof of concept scientific experiment and does not require a high revisit rate; therefore, any of the slewing options are acceptable.

The +/-8° slewing capability of the already selected dwell mirror allows CTEx to attain the highest level of simplicity by controlling all of the experiment's movement with one set of controllers and motors. This configuration was used for the remainder of

Table 4.1:   Sensor Parameters at Altitude

	Altitude	
	350 km	**450 km**
$FOV_{nadir}[km^2]$	0.293	0.484
$2R[m]$	610.9	785.4
$R[m]$	305.4	392.7
$FOV_{offnadir}[km^2]$	298.9	484.5
$2R[m]$	616.9	785.4
$R[m]$	308.4	392.7
$V_c[km/s]$	7.697	7.640
$T[min]$	91.538	93.586
$V_{gt}[km/s]$	7.297	7.137
$t_{nadirview}[s]$	0.0837	0.110
$\omega[deg/s]$	1.26	0.973

Table 4.2:   Target and Calibration Site Access

	Number of Accesses									
	0 deg		**8 deg**		**13 deg**		**18 deg**		**23 deg**	
	350 km	450 km	350 km	450 km	350 km	450 km	350 km	450 km	350 km	450 km
Dayton, OH	0	0	38	39	59	60	80	84	101	112
Mt. Wash., NH	0	0	39	47	62	76	87	108	117	140
Algeria 3	0	0	18	14	30	30	42	35	53	51
Algeria 5	0	0	10	12	19	27	26	35	33	51
Frenchman Flat	0	0	17	15	28	35	44	45	49	55
Libya 1	0	0	15	13	27	19	37	32	48	43
Libya 4	0	0	15	14	22	23	29	37	37	43
Mauritania 1	0	0	11	13	15	15	24	30	29	42
Mauritania 2	0	0	8	14	15	23	20	38	28	45

this research. Utilizing two controllers, one for each axis, for the dwell mirror maximizes precision. The dwell mirror in the telescope is capable of slewing +/- 8 degrees in each axis and achieves an acceptable number of accesses over both the target and calibration sites. All of the other options require the acquisition and integration of a rotation stage to control the cross-track slewing. This option increases complexity as well as places a potential strain on spatial constraints within the experiment housing.

4.2   Attitude Determination

This section covers the results of the attitude determination system analysis. The ISS's planned altitude of 450 km is used throughout the calculations and modeling within STK.

4.2.1   ISS Position and Attitude Accuracy.   Chapter III states that the attitude determination accuracy for the ISS is within +/- 3 degrees while the JAXA-KIBO module's accuracy is within 0.3 degrees. Table 4.3 shows the impact that these errors have on the target falling within the sensor's field of regard. The +/- 3 degrees of error in ISS attitude results in nearly a 33 percent reduction in the target falling within the field of regard of the sensor for two of the sites. Reducing this error to +/- 0.3 degrees yields less than a 10 percent reduction. The reduction percentages were calculated by taking the average of the reduced accesses for each attitude accuracy across all sites. Although this seems to be an acceptable level of performance, it is not. These statistics only show that a target will still fall within the field of regard, not the FOV. The following section discusses the accuracy required to ensure that a target actually falls within the FOV of CTEx.

4.2.2   Required Attitude Knowledge of CTEx.   CTEx has a small FOV, $R = 392$ m. Using Equations 3.1 and 3.2 at an altitude of 450 km and an off-Nadir angle of 8°, the diameters of the FOV of the sensor are approximately 785 m and 793 m at Nadir and 8° off Nadir respectively. The small FOV means that small error in the attitude will result in unacceptable pointing accuracy and no target acquisition. Equation 3.9 was

Table 4.3:   Impact of ISS Attitude Knowledge on CTEx Field of Regard

	Number of Accesses	Potentially Missed Accesses	
		+/-3 deg error	+/- 0.3 deg error
Dayton, OH	39	16	3
Mt. Wash., NH	47	17	0
Algeria 3	14	1	0
Algeria 5	12	5	0
Frenchman Flat	15	0	0
Libya 1	13	2	0
Libya 4	14	5	1
Mauritania 1	13	2	0
Mauritania 2	14	14	0

used to determine the pointing accuracy required to ensure that a target falls anywhere within the sensor's FOV.

$$\theta = \arctan\left(\frac{0.392km}{450km}\right) \cong .05deg = 180arcseconds \qquad (4.10)$$

This value of θ could result in the target being on the far edge of the FOV. However, the acceptable level of pointing accuracy required is half the radius of the FOV. Using the above equation where $R = 196m$ we solve for the acceptable pointing accuracy.

$$\theta = \arctan\left(\frac{0.196km}{450km}\right) \cong .025deg = 90arcseconds \qquad (4.11)$$

Increasing the precision of the pointing accuracy from 180 arcseconds to 90 arcseconds ensures that a target will lie within the central region of the FOV. This helps to limit the chance that system jitter will prevent target acquisition and data collection over the 10 second collection time.

4.2.3   Potential Attitude Determination Systems for CTEx.   The results of the previous section indicate that the pointing accuracy must be within 0.025 degrees or 90 arcseconds. Although the attitude accuracy is the dominant error, the accuracy of the slow steering or dwell mirror will have an impact as well. The telescope design incorporates two Aerotech ADRS-200 rotary stages with the specifications listed in Figure

4.1. The full technical specification for the rotary stage is provided in Appendix B. Two of the calibrated rotary stages have a combined accuracy of 14.1 arcseconds while the uncalibrated models have a combined accuracy of 113.1 arcseconds. Consequently, CTEx must use the calibrated model.

The calibration of the rotary stage is achieved by using an auto collimator and calculating the number of encoder counts that the rotary stage is off at each absolute angle. This information is then used to create a lookup table that is loaded into the controller. The incorporation of the lookup table removes much of the mechanical error out of the rotary stage.

Table 4.4 lists the commonly used options for the attitude determination hardware and their corresponding achievable accuracies. Immediately, all options with accuracies over 1 arcminute (or approximately 0.02 degrees) can be eliminated as possible options for CTEx.

4.2.4 Sun Sensors.   One possible hardware solution for attitude determination is the sun sensor. There are many companies that currently produce sun sensors with varying degrees of accuracy. Sun sensors require the addition of an inertial system since they only provide the pointing direction to the sun. Also, since the ISS does experience eclipse periods, CTEx will need to have a means of augmenting the attitude determination system during these periods if a sun sensor is selected. Figure 4.2 shows two of the sun sensors manufactured by The Netherlands Organization for Applied Scientific Research. There is no cost data for the sun sensors at this time.

Table 4.4:   Hardware Options for Attitude Determination[30]

Type	Obtainable Accuracy
Magnetometer	0.5 to 5.0 degrees
Horizon Sensor	5 arcminutes
Sun Sensor	1 arcminute
Solar Panel	1 degree
GPS	6 arcminutes
Star Tracker/Imager	<1 arcsecond

ADRS Series		ADRS-100		ADRS-150		ADRS-200	
Tabletop Diameter		95 mm		140 mm		190 mm	
Aperture		6 mm		15 mm		25 mm	
Motor (-A/-B)		S-76-35-A	S-76-35-B	S-130-39-A	S-130-39-B	S-180-44-A	S-180-44-B
Continuous Current, Stall	A_{pk}	2	4	3.8	7.6	2.7	5.3
	A_{rms}	1.4	2.8	2.7	5.4	1.9	3.8
Bus Voltage		320	160	320	160	320	160
Resolution		0.87-87.3 µrad (0.18-18 arc sec)		0.315-31.5 µrad (0.065-6.5 arc sec)			
Max Speed[1]		1500 rpm		600 rpm		400 rpm	
Accuracy	Uncalibrated	388 µrad (80 arc sec)					
	Calibrated[2]	29.1 µrad (6 arc sec)		48.5 µrad (10 arc sec)		48.5 µrad (10 arc sec)	
Repeatability		14.6 µrad (3 arc sec)		19.4 µrad (4 arc sec)		19.4 µrad (4 arc sec)	
Max Load[3]	Axial	7 kg		20 kg		40 kg	
	Radial	3 kg		10 kg		20 kg	
Axial Error Motion[4]		2 µm		5 µm		5 µm	
Radial Error Motion[4]		3 µm		5 µm		5 µm	
Tilt Error Motion		48.5 µrad (10 arc sec)		97 µrad (20 arc sec)		97 µrad (20 arc sec)	
Inertia	Unloaded	0.00038 kg-m²		0.00242 kg-m²		0.00843 kg-m²	
Total Mass		2.0 kg		4.3 kg		7.6 kg	
Finish	Tabletop	Hardcoat					
	Stage	Black Anodize					

Notes:
1. Maximum speed is based on stage capability. Actual speed may depend on encoder resolution, load, amplifier bus voltage, and motor. See the S-series rotary motor for more information.
2. With HALAR.
3. Maximum loads are mutually exclusive.
4. For the ADRS-100, error motion specifications are below 700 rpm. Above 700 rpm, the max radial error is 5 microns. Errors measured 50 mm (2 in) above the tabletop.

Figure 4.1:   Dwell Mirror Rotary Stage Specifications
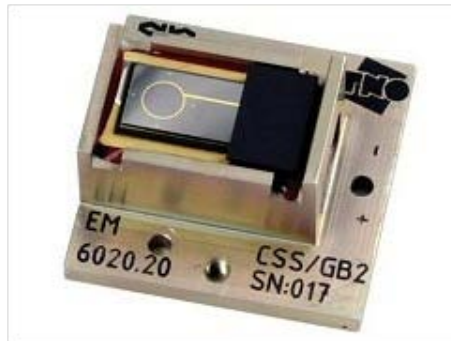
(a) Fine Sun Sensor (FSS)

(b) Cosine Sun Sensor (CoSS)

Figure 4.2:   TNO Sun Sensors[37, 38]

Fine Sun Sensor Instrument Specifications[37]: The FSS is a quadrant-based fine sun sensor that uses solar aspect angles over each of the four quadrants to determine position. The FSS has a bias error of less 0.3 arcseconds throughout its mission lifetime after implementation of ground calibration procedures. The instrument has an output voltage in the range of 0-5 V per quadrant, a noise equivalent angle less than 0.05^o and a resolution of less than 0.03^o. It has a reliability of more than 99.7% for a five year lifetime. The included alignment cube provides alignment accuracy of better than 0.05 arcseconds. The detector has a 3 mm glass cover shield for radiation protection.

- Mass: 375 g

- Dimensions: 108 x 106 x 49 mm^3

- Field of View: 138° x 138° unobstructed

- Power Consumption: <0.25 W

- Operating Temperature: -35^oC to $+70^oC$

Cosine Sun Sensor Instrument Specifications[38]: The CoSS is a radiation hard single photo diode with 300 μm thick coverglass and accuracy $\approx$ 3 arcseconds. CoSS has an output of $\approx$ 5 mA and a failure rate of 5 Failures in Time (FIT) at 50^oC with axis alignment to within 0.5 arcseconds. The term FIT is a unit of failure rate equal to the number of expected failures of a device in one billion operating hours.

- Mass: 24 g

- Dimensions: 30 x 30 x 14.5 mm^3

- Field of View: 160°, full cone angle

- Power Consumption: Passive

- Operating Temperature: -50^oC to $+85^oC$

4.2.5 Star Trackers.   The addition of a star tracker to CTEx will also serve as an option for attitude determination. A star tracker is the most accurate attitude determination system and there are several options available. Table 4.5 compares Terma's

HE-5AS Star Tracker, Surrey Satellite Technology's ALTAIR HB+ Star Tracker, Ball Aerospace and Technologies Corporation's CT-633 Star Tracker, COMTECH AeroAstro's Miniature Star Tracker (MST) and Sodern's SED-36. Three areas of significant interest are the accuracies, the cost, and the flight heritage. The ALTAIR HB+ and MST both have a significantly lower cost than the HE-5AS. The primary factor affecting the cost is the accuracy. Although all of the star trackers meet the accuracy requirement in the cross-boresight axes, the ALTAIR HB+ and MST exceed the total pointing accuracy requirement in the around-boresight axis. It is still possible to use either the ALTAIR HB+ or the MST, but a second star tracker is required to supplement the around-boresight axis of the first sensor. The apparent cost savings of the ALTAIR HB+ and MST over the HE-5AS is consumed by the need for an additional star tracker. Also of note is the lack of flight heritage for the MST. The other four star trackers have considerable heritage; the SED-36 is currently on the PLEIADES satellite, but its predecessor, SED-26, flew on SPOT5 and 57 other satellites.

4.3 Attitude Determination Recommendation

Section 4.2 shows that CTEx requires an attitude determination system separate from the systems already available on the ISS in order to meet pointing requirements. The information presented in Table 4.5 depicts the high level of accuracy available from the incorporation of a single star tracker. The recommendation has been made to incorporated the Terma HE-5AS star tracker due to its high level of accuracy and flight heritage. The $510K cost data does include all testing and calibration of the sensor. The Sodern SED-36 is also an acceptable choice based on accuracy and flight heritage; however, cost data must be obtained prior to a final decision on acceptability.

4.4 CTEx Mission Plan

This section covers an initial mission plan for CTEx. The plan begins with launch on 23 November 2012 and proceeds through data collection and downlinking. The launch date is a date selected at random to serve as a worst case starting point for this analysis. November is a worst case option because the seasons of the year do not align nicely with

Table 4.5: Star Tracker Comparison

	HE-5AS	ALTAIR HB+	CT-633	MST	SED-36
Attitude	3-axis attitude determination	3-axis attitude determination	3-axis attitude determination	3-axis attitude determination	3-axis attitude determination
Acquisition	autonomous 3-5 sec	autonomous 20-40 sec	autonomous < 60 sec	autonomous	autonomous < 4 sec
Stars Tracked		3-30	up to 5	up to 9	up to 14
Output data rate	1-4 Hz	0.5 Hz	5 Hz	2 Hz	1-8 Hz
Accuracy(cross boresight(BOL))	< 1 arcsecond	<30 arcseconds	4 arcseconds	< 35 arcseconds	< 1 arcseconds
Accuracy(around boresight(BOL))	< 5 arcsecond	<180 arcseconds	38 arcseconds	< 100 arcseconds	≈ 6 arcseconds
Heritage	Cryosat 1 and 2 Aeolus, LISA Pathfinder, Nemo Tacsat-1 and 2, Distributed Sensing Equipment, HREP	Bilsat-1 Beijing-1 CFESat Rapideye	Flyboy Impactor	Scheduled to fly 06/2010	PLEIADES
Cost	≈$510K	≈$205K		≈$250K	

the desired order of the experiments. Due to the timing, the three experiments outlined in Section 1.4 will require nearly nine months to complete. This section also assumes that CTEx, like HREP, will fly on the H-II Transfer Vehicle (HTV).

4.4.1 *From Launch to Installation on the JEM-EF.* It is reasonable to assume that CTEx will closely follow the same timeline that HREP followed. Table 4.6 shows the HREP timeline[32] modified for CTEx. The table shows the detailed timeline for launch, rendezvous with the ISS, docking with the ISS, and installation of the experiment on the JEM-EF. It will take eight days for CTEx to launch and reach the ISS. An additional three days is required to transfer equipment and supplies from the HTV to the ISS. Finally, on days 12 through 14, CTEx will be transferred from the Exposed Pallet (EP) to the appropriate location on the EF.

4.4.2 *Installation Complete to Calibration Complete.* Following installation of CTEx onto its specified port on the JEM-EF, initialization procedures must be run. The operating scheme of the instrument is depicted in the Appendix C. Figure C.1 shows the flow of inputs, actions, and outputs for the initialization and operation of CTEx. Figure C.2 depicts the functional verification testing flow that is run at startup top ensure that all of the subsystems are working properly and that the imager is calibrated. Figures C.3 and C.4 show the specific initialization procedures for the camera and encoder prior to data collection. Finally, Figure C.5 shows the initialization procedure for pointing and tracking a designated target with various levels of instrument autonomy.

Table 4.7 is the timeline from installation on the JEM-EF through the complete calibration of the system. Once CTEx is attached to the JEM-EF, the survival power will be turned on followed by the operational power. While powering on, the boot procedures and thermal configuration of the system is monitored. After successfully booting the system, the instrument will be taken out of launch configuration and placed into an operational configuration. Specifically, the mirrors and other mechanical components that are stabilized for launch must be released to enable a full range of motion. Next, the system is allowed to outgas for seven days. The seven day window was chosen as an initial estimation based on other similar sensors. However, once the final design is

52

Table 4.6:   CTEx Launch to Installation Timeline[32, 39]

	Year 2012	
Day	Date	Tasks
1	23 Nov	Launch/Insertion, post-insertion auto sequence (the HTV subsystem activations, attitude control, self-check, TDRS communications establishment, initiation of communication with the HTV Mission Control Room (MCR), TKSC, far field rendezvous flight maneuver
2	24 Nov	Far field rendezvous flight maneuver
3	25 Nov	Far field rendezvous flight demonstrations: Collision Avoidance Maneuver (CAM), passive abort and attitude control, correction from large attitude deviation, Free Drift
4-6	26-28 Nov	Far field rendezvous flight maneuver
7	29 Nov	IMMT review on the HTV demonstration operations data ; Arrival at the HTV PROX range
8	30 Nov	ISS proximity operations, final approach, capture by stations robotic arm, berthing to the ISS critical vestibule outfitting, activation of the HTV subsystems
9	1 Dec	Vestibule outfitting, crew ingress, cargo transfer (from HTV to ISS)
10-11	2-3 Dec	Cargo transfer from HTV to ISS
12	4 Dec	Temporary installation of the Exposed Pallet (EP) to Kibo Exposed Facility (EF)
13-14	5-6 Dec	Transfer and installation of CTEx to the Exposed Facility (EF)
15	7 Dec	Removal of the EP from the EF and reinstallation of the EP onto the HTV (robotic operation), transfer of waste and used materials from the ISS to the HTV (Inter-vehicular activity)

complete and a list of materials is available, the outgassing time will need to be calculated. While CTEx is outgassing, stray light within the system can be characterized and noise trending can be accomplished while all of the doors are still closed and the instrument is running.

On days 21 through 27, CTEx will conduct initial calibration, depicted in Figure 4.3. The pixel calibration and rough spectral calibration are both conducted with the aperture door closed. The pixel gain correction is accomplished using one of the six pseudo-invariant sites and averaging the pixel gains across the FPA. Next, an urban site is used to optimize the instrument focus. Finally, fine spectral calibration and radiometric calibration are completed using the Frenchman Flat site. These results will be downlinked to the ground site and analyzed at AFIT to ensure proper focus and calibration. Once these procedures are successfully completed, CTEx is prepared to conduct experiments and routine operations.

4.4.3 Mission Capable through Data Downlink. Once CTEx has successfully completed initial calibration, the data has been analyzed, and final settings have been uplinked to CTEx, the experiment will be considered mission capable. In this phase of operation CTEx will collect event data on a target of opportunity. A target of opportunity is defined as any target that requires no precise cross track slewing. The purpose of this collection is to test the in track motion compensation and evaluate the quality of data with all initial calibration corrections implemented. One possible means of collection is to conduct an absolute calibration shown in Figure 4.4 because these sites are large and uniform. Next, CTEx will conduct a data collection and downlink of a target requiring cross track slewing. This target should contain readily identifiable features to aid in geolocation of the image. This data will be analyzed on the ground to determine if the intended target was imaged, thus ensuring that the pointing system is working correctly. Finally, experimental data collections of the planned targets will be conducted, downlinked and analyzed.

STK provides some useful information on the revisit time for the sites used for absolute calibration. These are the same calibration sites listed in Table 3.1. The

Table 4.7:   CTEx Initialization

Day	Year 2012/13 Date	Tasks	Notes	Duration
14	6 Dec	CTEx Installed		
14	6 Dec	CTEx survival power on		
14	6 Dec	CTEx operational power on	Monitor boot and thermal configuration	2 d
15	7 Dec	CTEx exits launch configuration	Any implemented restraint or vibration damping materials are removed. CTEx is isolated from station vibrations	
16	8 Dec	Outgassing	Open CTEx detector door and outgas with dust covers closed	7 d
16	8 Dec	CTEx noise trending	Trend noise and search for light leaks with sensor CTEx sealed. Execute function test as shown in Appendix 3 w/o calibration. Dwell mirror will slew to max. deflection in both axes and reset to zero.	3 d
19	11 Dec	CTEx noise trending while CTEx is running	Characterize light leaks with CTEx sealed	1 d
21-27	13-19 Dec	Conduct initial calibration	Procedure depicted in Figure 4.3	7 d
28-43	20 Dec-4 Jan	Downlink calibration data	Data in downloaded and analyzed. Follow on commands for focusing are determined.	
50	11 Jan	CTEx parameters set	Focus and others commands executed. CTEx mission capable.	
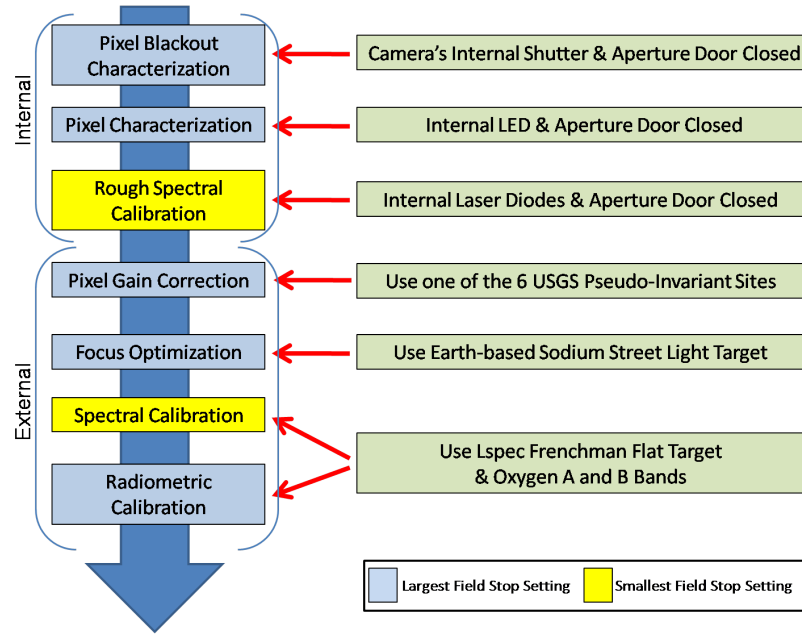
Figure 4.3:   CTEx Initial Calibration Flowchart.[35]

median revisit time for Frenchman Flat is 11 days while the minimum and maximum revisit times are four and 23 days respectively. The median revisit time for any one of the six pseudo-invariant sites is two days while the minimum and maximum revisit times are one and 10 days respectively. The median time between any one of the six pseudo-invariant sites and the next access of Frenchman Flat is six days while the minimum and maximum times are one and 16 days respectively. Table 4.8 outlines the timeline for this phase. These revisit times drive the planning window for calibration of the sensor to consume seven days.
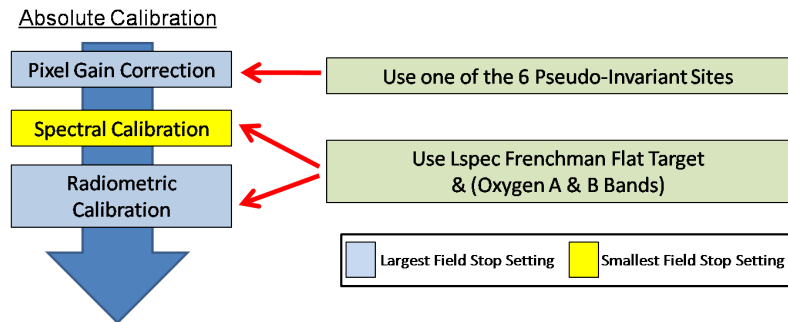
Figure 4.4:   CTEx Absolute Calibration Flowchart.[35] This procedure is conducted as required according to the results of calibration trending.

Table 4.8:   Verification of CTEx Function

	Year 2013			
Day	Date	Tasks	Notes	Duration
51-56	12-18 Jan	CTEx conducts absolute calibration	Calibration conducted as shown in Figure 4.4	7 d.
57	19 Jan	Calibration data downloaded	Data is downloaded via the high date rate	0.8 h
58-64	20-26 Jan	Calibration data analyzed	This data is used to validate CTEx alignment and focus. Initial pointing accuracy may be analyzed as well	7 d
65	27 Jan	Calibration Trending	Procedure shown in Figure 4.5	
79	10 Feb	Data collection	Collect data of a known location to validate pointing algorithm of CTEx	10 sec
80	11 Feb	Download data	Data is downloaded	0.8 h
81-84	12-15 Feb	Analyze data	Validate proper function of the pointing system through geolocation if image	4 d
91	21 Feb	Commands uploaded for first experiment		
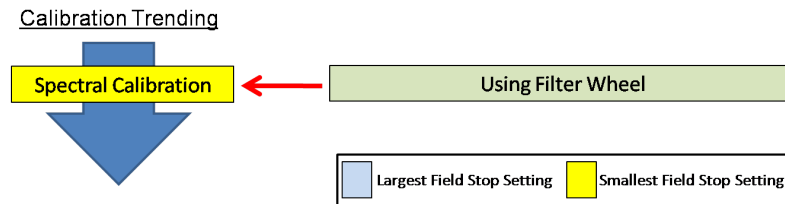
Figure 4.5:   CTEx Calibration Trending Flowchart.[35]

4.4.4   Conduct of Planned Experiments.   After the first 91 days in operation, CTEx will be fully initialized and calibrated and ready to collect data in accordance with the three experiments outlined in Section 1.4. The logical progression of events is the static hyperspectral scene, the large transient event, and the point source transient event as it follows the inherent progression of complexity. However, the target site locations of Dayton, OH and MT Washington, NH are comprised of primarily deciduous trees at low altitude. The absence of leaves in the months of February and March will require changing the order of experiments. Also, the large transient event is templated to be a forest fire or other large combustion event. The height of the forest fire season runs from mid to late summer. This again requires the order of experiments to change unless the launch date is changed to an early spring date. The new order of experiments is the point source transient event, the static hyperspectral scene, and the large transient event. Tables 4.9 and 4.10 highlight the major events associated with the conduct of the three experiments.

It is important to note that the timeline does not show every iteration of routine events. As discussed in Section 2.5, there is a daily submission to, or confirmation with, NASA of future commands that the satellite will execute. Also, the instrument will execute calibration trending on a daily basis to determine when an absolute calibration is required. For planning purposes it is expected that an absolute calibration will need to be conducted on a monthly basis. CTEx will also execute routine commands such as downlinking health information.

The point source transient event collection can be established at either target location. Each site experiences an average of 25 days of clear or partly cloudy days during the month of March.[40] Using the STK simulation, it was determined that the Dayton, OH and MT Washington, NH will be visible for five days and seven days respectively during the month of March. The initial experiment was planned for 6 Mar at MT Washington, NH, but the cloud cover was too thick and the secondary collection was accomplished on 7 Mar at MT Washington, NH.

The static hyperspectral scene can be accomplished at either Dayton, OH or MT Washington, NH. In this simulation, the experiment takes place at Dayton, OH and has

a primary and secondary collection opportunity planned for 12 Apr. This experiment consists of imaging a specific location in an effort to discriminate a camouflaged vehicle from surrounding vegetation.

There is a break in the timeline between the static hyperspectral experiment and the large transient experiment. This break is due to the time of the year and the low probability that there will be a forest fire prior to the summer months. This time period can be used to repeat other experiments or to execute collections on targets of opportunity not discussed in this thesis.

The site of the large transient event was arbitrarily chosen to be a historic site of the fires located to the Northeast of Los Angeles, CA in the Angeles National Forest. During the months of July and August, the Angeles National Forest is accessible to CTEx a total of eight times. The combination of the intermittent clouds and the smoke from the fire may hinder collection slightly, but the long window for collection increases success.

The data downlink times depicted in the planning timeline are based on the high data rates of the JEM shown in Figure 2.12. It is assumed that CTEx will image at 1000 frames per second, use a FPA area of 1024 by 1024 pixels, and collect ten seconds of data that needs to be transmitted. The shared 34 Mbps high-rate data results in a downlink time of approximately 48 minutes. If CTEx is constrained to using the low-rate data, then the downlink time increases to just over 34 hours. Consequently, CTEx will require use of the high-rate data for downlink of experimental data. Routine data can be sent using the low-rate data.

4.5 Summary

As mentioned earlier, this is a worst case scenario analysis with a November launch date. It will take approximately 15 days from launch until CTEx is installed on the JEM-EF; the initialization of the instrument will take approximately 35 days; the initial data collection and characterization of the system will take approximately 40 days. Assuming results are favorable at the conclusion of the first 91 days, CTEx will be capable of providing reliable data for any of the three experiments discussed in Section 1.4. The

59

Table 4.9:   Planned Experiment Execution

Day	Date	Tasks	Notes	Duration
	Year 2013			
91-97	21-28 Feb	CTEx conducts absolute calibration	Calibration conducted as shown in Figure 4.4	7 d.
103	6 Mar	Point source transient event	Cloud cover too thick switch to secondary collection opportunity	
104	7 Mar	Point source transient event	Collection successful. Prepare to downlink	10 sec
105	8 Mar	Downlink data	Data downlink via high data rate	0.8 h
105-111	8-14 Mar	Analyze data for transient event	Data analyzed for spatial and spectral content and determine if experiment needs to be repeated	7 d
105	8 Mar	Submit commands for absolute calibration	3 weeks out	
119	22 Mar	Submit commands for static hyperspectral event	3 weeks out	
119	22 Mar	Confirm commands for absolute calibration	1 week out	
123	26 Mar	Confirm commands for absolute calibration	3 days out	
126	29 Mar	Execute commands for absolute calibration		5 d
134	5 Apr	Confirm commands for static hyperspectral event	1 week out	
137	9 Apr	Confirm commands for static hyperspectral event	3 days out	
139	11 Apr	Conduct calibration trending		1 h
140	12 Apr	Execute commands for static hyperspectral event	Tank in the trees experiment	10 sec
141	13 Apr	Downlink data	Data downlink via high data rate	0.8 h
141-148	13-19 Apr	Analyze data for static hyperspectral event	Data analyzed for spatial and spectral content and determine if experiment needs to be repeated	7 d

Table 4.10:   Planned Experiment Execution Continued

| | Year 2013 | | | |
Day	Date	Tasks	Notes	Duration
230	10 Jul	Submit commands for absolute calibration	3 weeks out	
237	17 Jul	Submit commands for large transient event	3 weeks out	
244	24 Jul	Confirm commands for absolute calibration	1 week out	
248	28 Jul	Confirm commands for absolute calibration	3 days out	
251	31 Jul	Execute commands for absolute calibration		6 d
252	1 Aug	Confirm commands for large transient event	1 week out	
255	4 Aug	Confirm commands for large transient event	3 days out	
257	6 Aug	Conduct calibration trending		1 h
258	7 Aug	Execute commands for large transient event	Angeles National Forest fire experiment	10 sec
259	8 Aug	Downlink data	Data downlink via high data rate	0.8 h
259-265	15 Aug	Analyze data for static hyperspectral event	Data analyzed for spatial and spectral content and determine if experiment needs to be repeated	7 d

three experiments will take approximately 170 days to complete given a launch date in November. This timeline is primarily driven by the conditions required to execute each of the three experiments. The large transient event, a forest fire, requires that it be fire season. The primary plan for a large fire should be to plan a controlled burn. Controlled burns occur on a regular basis on Army installations and throughout the forestry service. The back-up plan should be to image naturally occurring fires. These natural fires may provide several data collection opportunities in addition to any planned controlled burns. The point source transient event can be conducted at any time of the year. The static hyperspectral scene requires that there be sufficient naturally occurring vegetation to render a man-made object indistinguishable from the surroundings to the naked eye. Although this timeline is significant, it is not unreasonable to request an on-orbit life of one year for a JEM-EF payload.

Perhaps the most important planning factor in accomplishing the three experiments within the NASA planning scheme is the programming of multiple target collection opportunities for each experiment. Programming for and collecting against multiple targets for a single experiment will increase the probability of a successful experiment given possible pointing errors and cloud cover over the targets. Of course this requires sufficient data storage capabilities and increases the desire to have some form of on-board processing that can, at least, determine if the target was detected during the collection opportunity.

V. Conclusions

5.1 Summary of Thesis

Chapters I and II discuss the background information that is pertinent to understanding the utility of CTEx and chromotomography is general. Several examples of currently operational hyperspectral imagers are discussed to determine how elements of their design can be utilized for CTEx. Also, by comparison with these imagers, the enhanced capabilities of CTEx are presented. The theory behind CTEx is presented to demonstrate the capability that CTEx provides to collect spatial and spectral information of very transient events such as detonations.

Chapter III presents the methodology for determining the slewing, Section 3.1, and attitude determination, Section 3.3, requirements for CTEx and presents all relevant equations. Section 3.1.2 outlines the process for building the STK simulation: defining the parameters for the sensor FOV, establishing the sensor's location on the ISS, and creating the two target sites and seven calibration site locations.

Chapter IV details the results of the research and the analysis of those results. The analysis is conducted by constructing a concept of operations, Section 4.4, for CTEx from launch to collection and analysis of experimental data. As discussed in Chapter IV, this concept of operations is a worst case scenario which still accomplishes all planned experiments. The total time required to execute a thorough initialization, calibration, and characterization of CTEx and to conduct the experiments is nearly nine months if the launch date is in the Winter. This timeline can easily be shortened by either moving the launch date to the Spring or redefining the experiments to make them less dependent upon climatological factors.

5.2 Recommendations for Future Research

This thesis is a study of slewing and attitude determination requirements for CTEx given the 0.05^o sensor half-angle, the most restrictive FOV for the system. The evolving design of the instrument now incorporates an adjustable field stop that will provide the capability of adjusting this half-angle. The access rates and acceptable pointing accuracy for the additional half-angles have not been analyzed. Analysis of the additional

FOVs will provide insight into the optimal operating parameters for calibration and data collection given specific spatial and spectral resolution requirements.

Also, once the actual telescope and CTEx instrument is built there will be a need for substantial testing. Specifically, there is no data on the amplitude and frequency of the system jitter. The motors for the mirrors and prism encoder as well as the field stop actuator will introduce jitter into the system. No work has been done to correct for jitter to ensure that it is possible to collect usable data.

Perhaps the most substantial area of future research is development of the software to tie the pointing and attitude determination systems together. The extremely small FOV of CTEx requires that the pointing system receive updated attitude information and determine the proper azimuth and elevation to slew the dwell mirror given the target location on the Earth. The calculations must be accomplished on-board CTEx due to attitude prediction inaccuracies and the command upload timeline. There is very little chance that CTEx can image a specified point target without a reliable and efficient software package.

As the design of the space-based instrument matures and specific hardware is selected, the mission plan will require much refinement. The data cube size and associate data analysis algorithms will dictate the downlink time for each event. There is certainly a research opportunity in developing an on-board pre-processing algorithm to detect scene anomalies and package those frames for downlink.

5.3   Conclusions

CTEx provides the capabilities required to enhance exploitation of spatial and spectral data from fast transient events and serves as a proof of concept experiment that will revolutionize hyperspectral remote sensing. This thesis examines the strict requirements for pointing CTEx and the associated factors that require CTEx to operate with a high degree of autonomy. Although there are several challenges in designing and operating a hyperspectral imager with an extremely small FOV on-board the ISS, the demonstration of the capabilities of CTEx will directly impact the warfighter and

civilian community by creating the ability to characterize spectrally transient events from a space-based platform.

Appendix A. Hyperspectral Imagers[1]

5.1   AIRBORNE / SPACEBORNE SYSTEMS [1,9]

Name	Full Name	Manufacturer Country	Number of Bands	Spectral Range (μm)	Band Width at FWHM (nm)
AAHIS	Advanced Airborne Hyperspectral Imaging System	SETS Technology	288	0.432 – 0.832	6
AHI	Airborne Hyperspectral Imager	Hawaii Institute of Geophysics and Planetology	256	7.5 – 11.7	100
AHS	Airborne Hyperspectral Scanner	Daedalus Enterprise Inc.	48	0.433 – 12.70	
AIP	Airborne Instrument Program	Lockheed USA		2.00 – 6.40	
AIS-1	Airborne Imaging Spectrometer	NASA, JPL USA	128	0.90 – 2.10 1.20 – 2.40	9.3 10.6
AMSS	Airborne Multispectral Scanner MK-II	Geoscan Pty Ltd.	46	0.50 – 12.00	
ARES		USA	75	2.00 – 6.50	
ARIES	Australian Resource Information and Environment Satellite	Australia	128	0.40 – 2.50	
APEX	Airborne Prism Experiment		Programmable to a max of 300	0.38 – 2.50	10
CHRISS	Compact High Resolution Imaging Spectrograph Sensor	Science Applications Int. Corp. (SAIC) USA	40	0.43 – 0.87	
CIS	Chinese Imaging Spectrometer	Shanghai Institute of Technical Physics China	91	0.40 – 12.50	
DAIS 21115	Digital Airborne Imaging Spectrometer	GER Corp. Germany	211	0.40 – 12.00	
DAIS 3715	Digital Airborne Imaging Spectrometer	GER Corp. Germany	37	0.40 – 12.00	
DAIS 7915	Digital Airborne Imaging Spectrometer	GER Corp. Germany	79	0.40 – 12.00	
DAIS 16115	Digital Airborne Imaging Spectrometer	GER Corp. Germany	160	0.40 – 12.00	

Name	Full Name	Manufacturer Country	Number of Bands	Spectral Range (μm)	Band Width at FWHM (nm)
EART EXPLORER		ESA	202 (?)	(3)10 – 1000	
EO-1		USA	7	0.43 – 2.35	
EPS-A	Environmental Probe System	Germany	32	0.40 – 12.00	
EPS-H	Environmental Probe System	Germany	76 * 32 32 12	0.43 – 1.05 * 1.50 – 1.80 2.00 – 2.50 8.00 – 12.00	*Customised according user requirements
FLI/PMI	Fluorescence Line Imager / Programmable Multispectral Imager	Moniteq Ltd.	228	0.43 – 0.805	
FTVFHSI	Fourier Transform Visible Hyperspectral Imager	Kestrel Corp., FIT	256	0.44 – 1.15	
GERIS	Geophysical and Environmental Research Imaging Spectrometer	Germany	63	0.40 – 2.50	
HIRIS	High Resolution Imaging Spectrometer	USA	192	0.40 – 2.50	
HYDICE	Hyperspectral Digital Imagery Collection Experiment	USA	210	0.40 – 2.50	7.6 – 14.9
HYMAP		Integrated Spectronics Australia	126	0.45 – 2.50	15 – 20
HYPERION		TRW	220	0.40 – 2.5	10
IISRB	Infrared Imaging Spectrometer	Bomen	1720	3.50 – 5.00	
IMSS	Image Multispectral Sensing	Pacific Advanced Technology	320	2.00 – 5.00	
IRIS	Infrared Imaging Spectrometer	ERIM USA	256	2.00 – 15.00	
ISM	Imaging Spectroscopic Mapper	DESPA	128	0.80 – 3.20	
LIVTIRS 1	Livermore Imaging Fourier Imaging Spectrometer	Lawrence Livermore USA		3.00 – 5.00	

Name	Full Name	Manufacturer Country	Number of Bands	Spectral Range (μm)	Band Width at FWHM (nm)
LIVTIRS 2	Livermore Imaging Fourier Imaging Spectrometer	Lawrence Livermore USA		8.00 – 12.00	
MAIS	Modular Airborne Imaging System	Shanghai Institute of Technical Physics China	71	0.44 – 11.8	
MAS	Modis Airborne Simulator	Daedalus Enterprise Inc. USA	50	0.53 – 14.50	
MERIS	Medium Resolution Imaging Spectrometer	ESA	15	0.40 – 1.05	
MIDIS	Multiband Identification and Discrimination Imaging Spectroradiometer	Surface Optics Corp., JPL, USA	256	0.40 – 30.00	
MIVIS	Multispectral Infrared and Visible Imaging Spectrometer	Daedalus Enterprise Inc. USA	102	0.43 – 12.70	
MODIS	Moderate Resolution Imaging Spectrometer	NASA USA	36	0.41 – 14.24	
OMIS	Operative Modular Airborne Imaging Spectrometer		128	0.46 – 12.50	
PROBE-1			100 – 200	0.44 – 2.54	11 – 18
ROSIS	Reflective Optics System Imaging Spectrometer	DLR, GKSS, MBB Germany	128	0.45 – 0.85	5
SASI	Shortwave Infrared Airborne Spectrographic Sensor		160	0.85 – 2.45	10
SFSI	SWIR Full Spectrographic Imager	CCRS Canada	122	1.20 – 2.40	10.3
SMIFTS	Spatially modulated Imaging Fourier Transform	Hawaii Institute of Geophysics USA	75	1.00 – 5.00	
SSTI HSI	Small Satellite Technology Initiative Hyperspectral Imager	TRW Inc. USA	384	0.40 – 2.50	
TRWIS III	TRW Imaging Spectrometer	TRW Inc USA.	384	0.30 – 2.50	

Name	Full Name	Manufacturer Country	Number of Bands	Spectral Range (μm)	Band Width at FWHM (nm)
VIFIS	Variable Interference Filter Imaging Spectrometer	University of Dundee	60	0.44 – 0.89	10
VIMS-V	Visible Infrared Mapping Spectrometer	ASI	512	0.30 – 1.05	
WIS	Wedge Imaging Spectrometer	Hughes St. Barbara Research Center USA	170	0.40 – 2.50	
WARFIGHTER (WF-1)		Phillips Laboratory USA	280	0.45 – 5.00	

5.2   GROUND BASED / HAND HELD SYSTEMS

Name	Manufacturer Country	Number of Bands	Spectral Range (μm)	Technology
GALAAD (Prototype)	ATIS France		7.0 – 14.0	Double grating with needle mask
CTHIS LWIR (CromoTomographic Hyperspectral Imaging Spectrometer)	Solid State Scientific Corporation USA	40	6.5 – 11.0	Rotating prism
CTHIS MWIR (CromoTomographic Hyperspectral Imaging Spectrometer)	Solid State Scientific Corporation USA	64	2.7 – 5.0	Rotating prism
ImSpector N10	Spectral Imaging Ltd. (Specim) Finland	Spectral resol 5.0 nm	0.7 – 1.0	Prism-Grating-Prism (PGP)
ImSpector N17	Spectral Imaging Ltd. (Specim) Finland	Spectral resol 10.0 nm	0.9 – 1.75	Prism-Grating-Prism (PGP)
Orion IR Multispectral Imager (SWIR, MWIR, LWIR models)	CEDIP France	4 or 6 per model	SWIR MWIR LWIR customized	Filter wheel

Name	Manufacturer Country	Number of Bands	Spectral Range (μm)	Technology
Sherlock LWIR	Pacific Advanced Technology USA	Spectral resol. 3 nm at $\lambda = 3.0\mu$m	8.0 – 10.5	IMSS (Image Multi Spectral Sensing)
Sherlock MWIR	Pacific Advanced Technology USA	Spectral resol. 33 nm at $\lambda = 8.0\mu$m	3.0 – 5.0	IMSS (Image Multi Spectral Sensing)

Appendix B. ADRS Rotary Stage Data Sheet[2]

ADRS Series

Mechanical-Bearing Rotary Stage

High torque output, direct-drive brushless servomotor

Cog-free slotless motor design for outstanding velocity stability

Direct coupled, high-accuracy rotary encoder

Ultra-low-profile minimizes working height

Aerotech's ADRS series with its direct-drive technology and low profile provide a superior alternative to belt- and worm-drive stages.

Compact Package

The design of the ADRS series direct-drive rotary stage was optimized to minimize stage height. The low profile of the stage reduces the effective working height of the system minimizing "stack-up" related errors. In addition to the low overall height, the ADRS series provides a clear aperture that can be used for product feed-through or laser beam delivery.

Brushless Direct-Drive

To maximize positioning performance, the ADRS series utilizes direct-drive brushless motor technology. Direct-drive technology is optimized for 24/7 production environments, as there are no brushes to replace and no gear trains or belts to maintain. Direct drive also provides quicker acceleration and higher top speeds than gear- or belt-driven mechanisms, yielding higher total overall throughput.

The low maintenance and high-throughput characteristics of the ADRS series provide a stage that yields the lowest total cost of ownership.

Slotless Motor

The ADRS series uses a slotless stator design that eliminates torque ripple. This motor technology provides ultra-smooth velocity stability comparable to a high-quality DC brush motor without all the DC motor's inherent maintenance requirements. Since the slotless motor is directly coupled to the tabletop, velocity disturbances created by toothed belt drives or worm gears are eliminated.

Multiple Configurations

The ADRS series is available in 100 mm, 150 mm, and 200 mm versions. Each stage has options for different motor windings to better match the stage to different operating conditions. The -B winding option provides the highest possible speed operation for a given available bus voltage, while the -A winding gives greater output torque for comparable current levels. Metric and "English" pattern tabletops are available and slotted mounting holes enable attachment to 25 mm and 1inch hole pattern breadboards. The tabletop of the ADRS series has a labyrinth seal that protects the bearings and encoder from contamination. An optional shaft end seal is available for applications where the bottom of the stage is exposed to contamination.

Axial and Radial Cantilevered Load Capability (ADRS100)
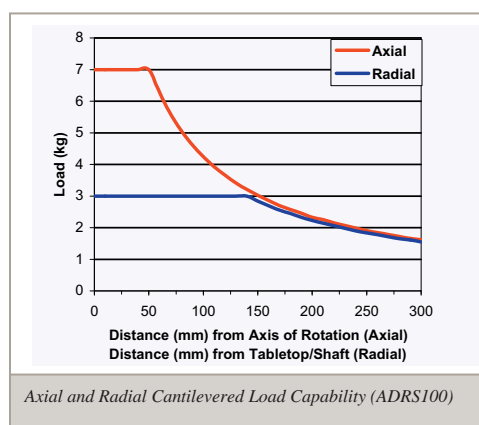
ADRS Series SPECIFICATIONS

ADRS Series		ADRS-100		ADRS-150		ADRS-200	
Tabletop Diameter		95 mm		140 mm		190 mm	
Aperture		6 mm		15 mm		25 mm	
Motor (-A/-B)		S-76-35-A	S-76-35-B	S-130-39-A	S-130-39-B	S-180-44-A	S-180-44-B
Continuous Current, Stall	A_{pk}	2	4	3.8	7.6	2.7	5.3
	A_{rms}	1.4	2.8	2.7	5.4	1.9	3.8
Bus Voltage		320	160	320	160	320	160
Resolution		0.87-87.3 µrad (0.18-18 arc sec)		0.315-31.5 µrad (0.065-6.5 arc sec)			
Max Speed[1]		1500 rpm		600 rpm		400 rpm	
Accuracy	Uncalibrated	388 µrad (80 arc sec)					
	Calibrated[2]	29.1 µrad (6 arc sec)		48.5 µrad (10 arc sec)		48.5 µrad (10 arc sec)	
Repeatability		14.6 µrad (3 arc sec)		19.4 µrad (4 arc sec)		19.4 µrad (4 arc sec)	
Max Load[3]	Axial	7 kg		20 kg		40 kg	
	Radial	3 kg		10 kg		20 kg	
Axial Error Motion[4]		2 µm		5 µm		5 µm	
Radial Error Motion[4]		3 µm		5 µm		5 µm	
Tilt Error Motion		48.5 µrad (10 arc sec)		97 µrad (20 arc sec)		97 µrad (20 arc sec)	
Inertia	Unloaded	0.00038 kg-m^2		0.00242 kg-m^2		0.00843 kg-m^2	
Total Mass		2.0 kg		4.3 kg		7.6 kg	
Finish	Tabletop	Hardcoat					
	Stage	Black Anodize					

Notes:
1. Maximum speed is based on stage capability. Actual speed may depend on encoder resolution, load, amplifier bus voltage, and motor. See the S-series rotary motor for more information.
2. With HALAR.
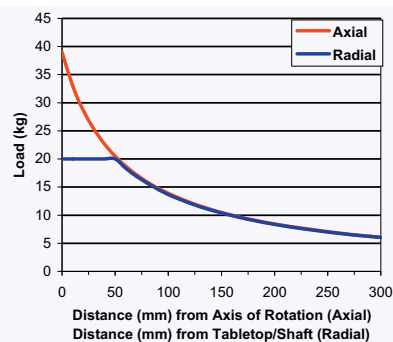3. Maximum loads are mutually exclusive.
4. For the ADRS-100, error motion specifications are below 700 rpm. Above 700 rpm, the max radial error is 5 microns. Errors measured 50 mm (2 in) above the tabletop.

ADRS Maximum Encoder Frequency

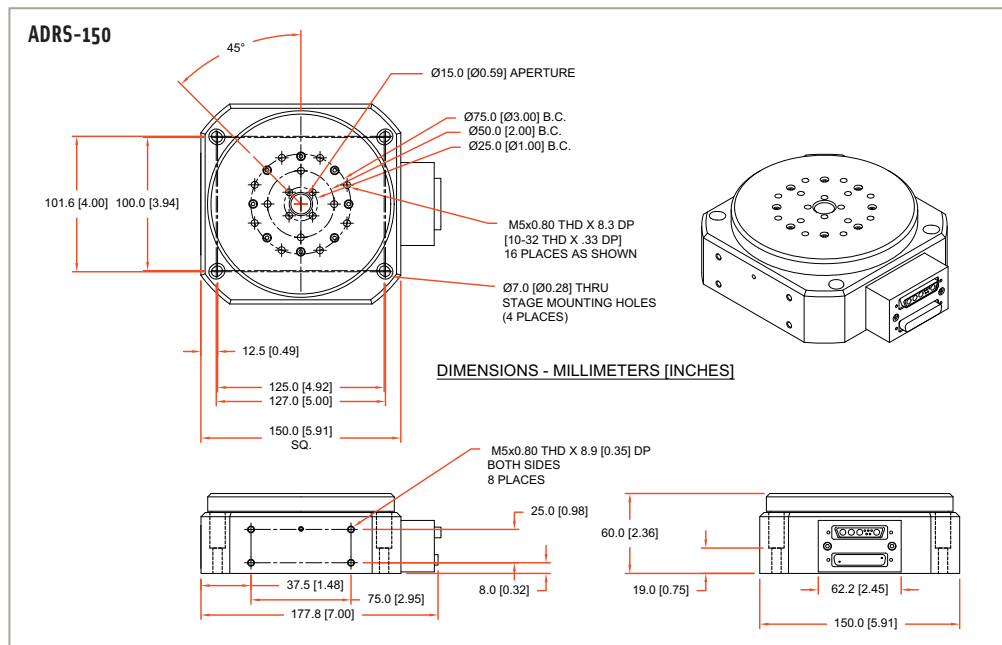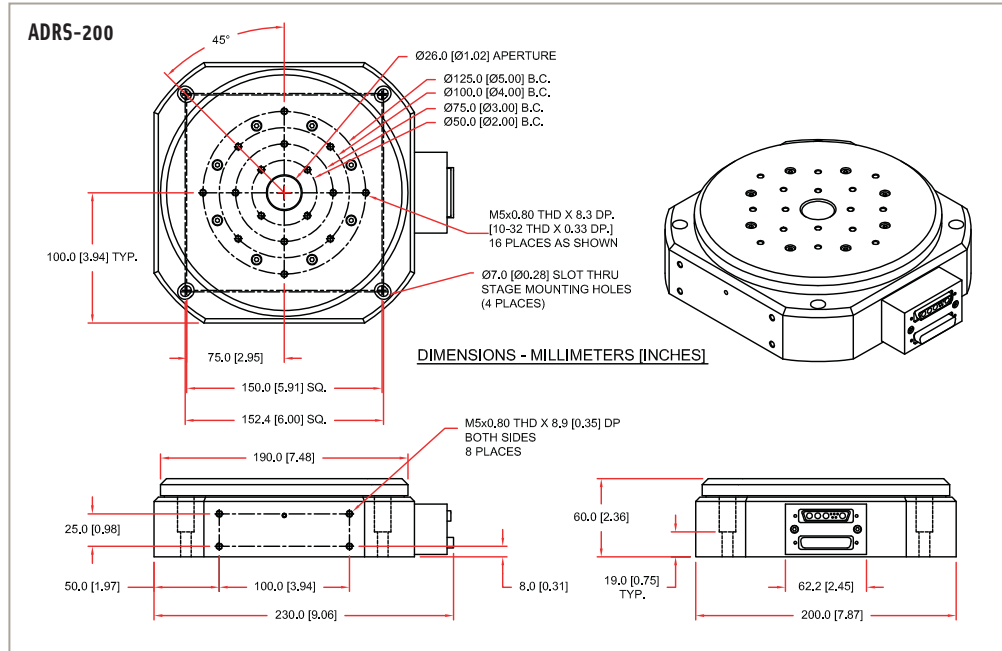| Resolution-Speed	ADRS-100	ADRS-150	ADRS-200
AS/X5/X10	1500 rpm	600 rpm	600 rpm
X25	1067 rpm	384 rpm	384 rpm
X50	533 rpm	192 rpm	192 rpm
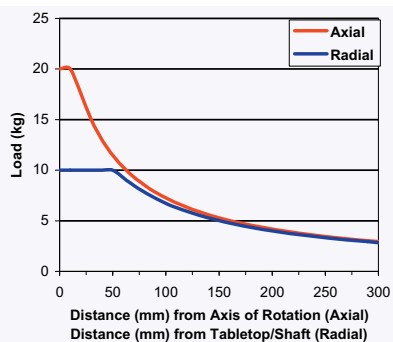
Axial and Radial Cantilevered Load Capability (ADRS150)

Axial and Radial Cantilevered Load Capability (ADRS200)

www.aerotech.com

ADRS Series DIMENSIONS

ADRS-200

45°

Ø26.0 [Ø1.02] APERTURE

Ø125.0 [Ø5.00] B.C.
Ø100.0 [Ø4.00] B.C.
Ø75.0 [Ø3.00] B.C.
Ø50.0 [Ø2.00] B.C.

M5x0.80 THD X 8.3 DP.
[10-32 THD X 0.33 DP.]
16 PLACES AS SHOWN

Ø7.0 [Ø0.28] SLOT THRU
STAGE MOUNTING HOLES
(4 PLACES)

100.0 [3.94] TYP.

75.0 [2.95]

DIMENSIONS - MILLIMETERS [INCHES]

150.0 [5.91] SQ.

152.4 [6.00] SQ.

M5x0.80 THD X 8.9 [0.35] DP
BOTH SIDES
8 PLACES

190.0 [7.48]

25.0 [0.98]

60.0 [2.36]

50.0 [1.97]

100.0 [3.94]

8.0 [0.31]

19.0 [0.75]
TYP.

62.2 [2.45]

230.0 [9.06]

200.0 [7.87]

ADRS-150

45°

Ø15.0 [Ø0.59] APERTURE

Ø75.0 [Ø3.00] B.C.
Ø50.0 [2.00] B.C.
Ø25.0 [Ø1.00] B.C.

M5x0.80 THD X 8.3 DP
[10-32 THD X .33 DP]
16 PLACES AS SHOWN

Ø7.0 [Ø0.28] THRU
STAGE MOUNTING HOLES
(4 PLACES)

101.6 [4.00]   100.0 [3.94]

12.5 [0.49]

DIMENSIONS - MILLIMETERS [INCHES]

125.0 [4.92]
127.0 [5.00]

150.0 [5.91]
SQ.

M5x0.80 THD X 8.9 [0.35] DP
BOTH SIDES
8 PLACES

25.0 [0.98]

60.0 [2.36]

37.5 [1.48]

75.0 [2.95]

8.0 [0.32]

19.0 [0.75]

62.2 [2.45]

177.8 [7.00]

150.0 [5.91]

ADRS Series DIMENSIONS and ORDERING INFORMATION

ADRS-100

Ø6.0 [Ø0.24] APERTURE

M4 x 0.70 THD X 6.3 DP
[8-32 THD X .25 DP]
5 PLACES AS SHOWN

50.0 [2.00] SQ.

Ø7.0 [Ø0.28] THRU
STAGE MOUNTING HOLES
(4 PLACES)

75.0 [2.95] SQ.
76.2 [3.00] SQ.

DIMENSIONS - MILLIMETERS [INCHES]

95.0 [3.74]

M5x0.80 THD X 8.9 [0.35] DP
BOTH SIDES
8 PLACES

25.0 [0.98]

55.0 [2.17]

8.0 [0.31]

50.0 [1.97]

130.0 [5.12]

19.0 [0.75]

62.2 [2.45]

100.0 [3.94]
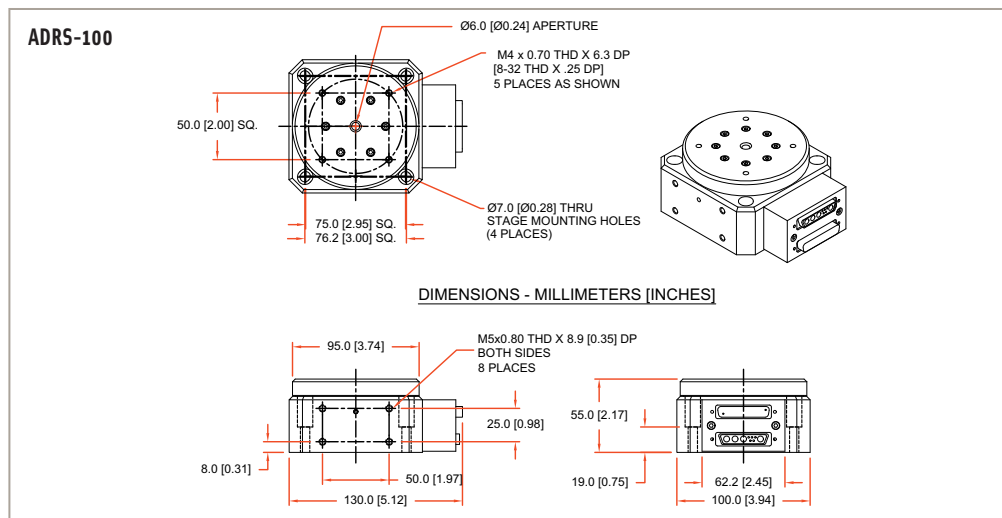
Ordering Example

ADRS	-200	-M	-A	-AS	-S
Series	Width (mm)	Mounting Pattern	Winding Option	Position Transducer	Construction Options
	-100	-M	-A	-AS	-S
	-150	-U	-B	-X	
	-200				

ADRS Series Direct-Drive Rotary Stage

ADRS-100	100 mm wide direct-drive rotary stage with 1.8 N-m peak torque output
ADRS-150	150 mm wide direct-drive rotary stage with 11.7 N-m peak torque output
ADRS-200	200 mm wide direct-drive rotary stage with 30 N-m peak torque output

Mounting Pattern

-M Metric-dimension mounting pattern and holes
-U English-dimension mounting pattern and holes

Winding Options

-A Low speed, high torque-constant winding option
-B High speed, low torque-constant winding option

Position Transducer

-AS Standard feedback device, 1 Vpp sine wave output, 10,000 cycles per rev on ADRS-200/150, 3600 cycles per rev on ADRS-100
-X5 Square wave digital output, 50,000 cycles per rev on ADRS-200/150 and 18,000 cycles per rev on ADRS-100
-X10 Square wave digital output, 100,000 cycles per rev on ADRS-200/150 and 36,000 cycles per rev on ADRS-100
-X25 Square wave digital output, 250,000 cycles per rev on ADRS-200/150 and 90,000 cycles per rev on ADRS-100
-X50 Square wave digital output, 500,000 cycles per rev on ADRS-200/150 and 180,000 cycles per rev on ADRS-100

Note: Digital output encoder signals are synthesized with a 16 MHz clock. Care must be taken to ensure that the encoder sample rate on the controller is at least 16 MHz or higher. Slower clock rates are available on request.

Construction Options (ADRS 150 & 200)

-S Bottom shaft seal (not available on ADRS-100; ADRS-100 has an integral bottom labyrinth seal)
-NS No bottom shaft seal

www.aerotech.com

Appendix C. Software Flow Charts for CTEx Functions[3]
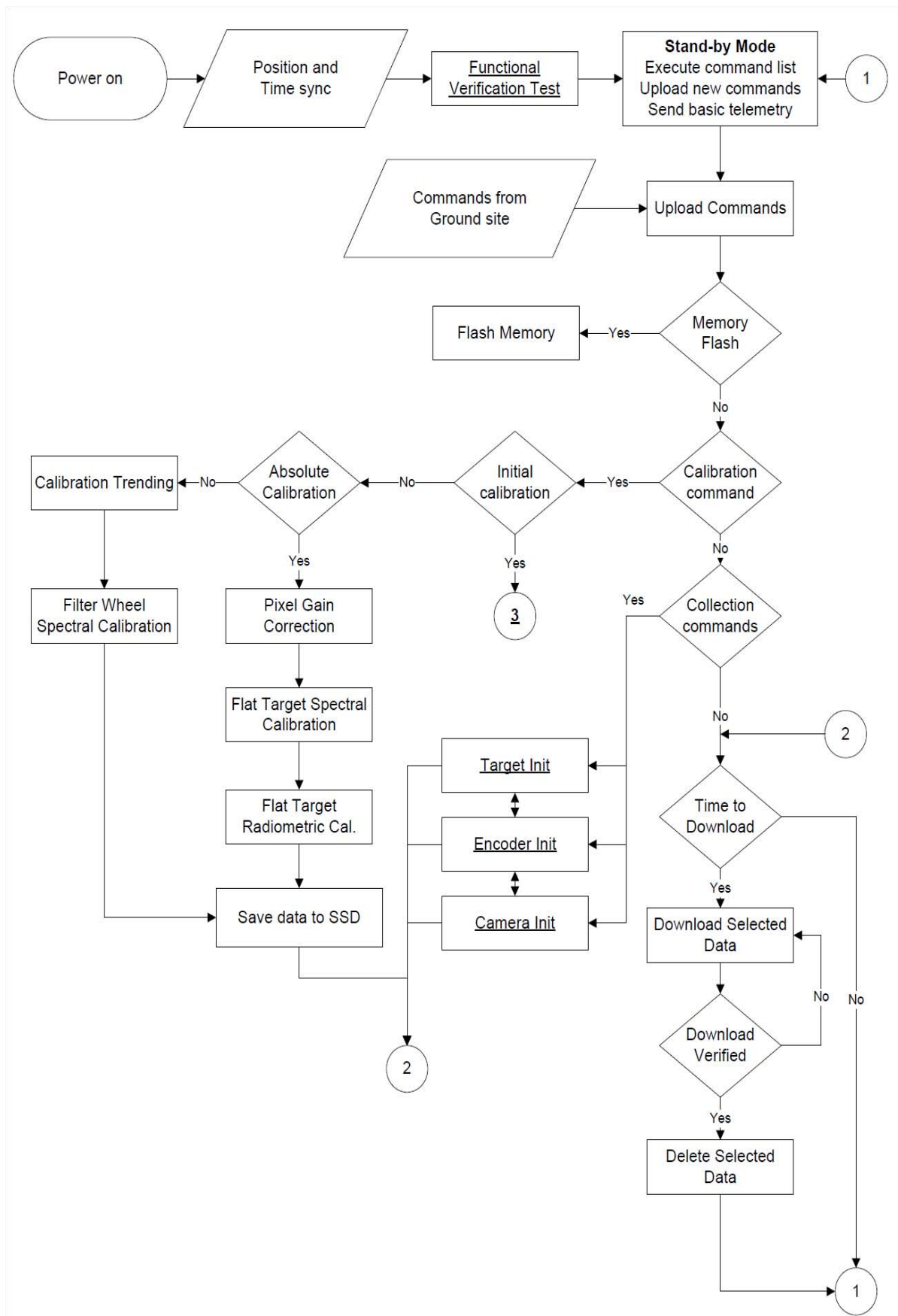
Figure C.1:   Overall Operation
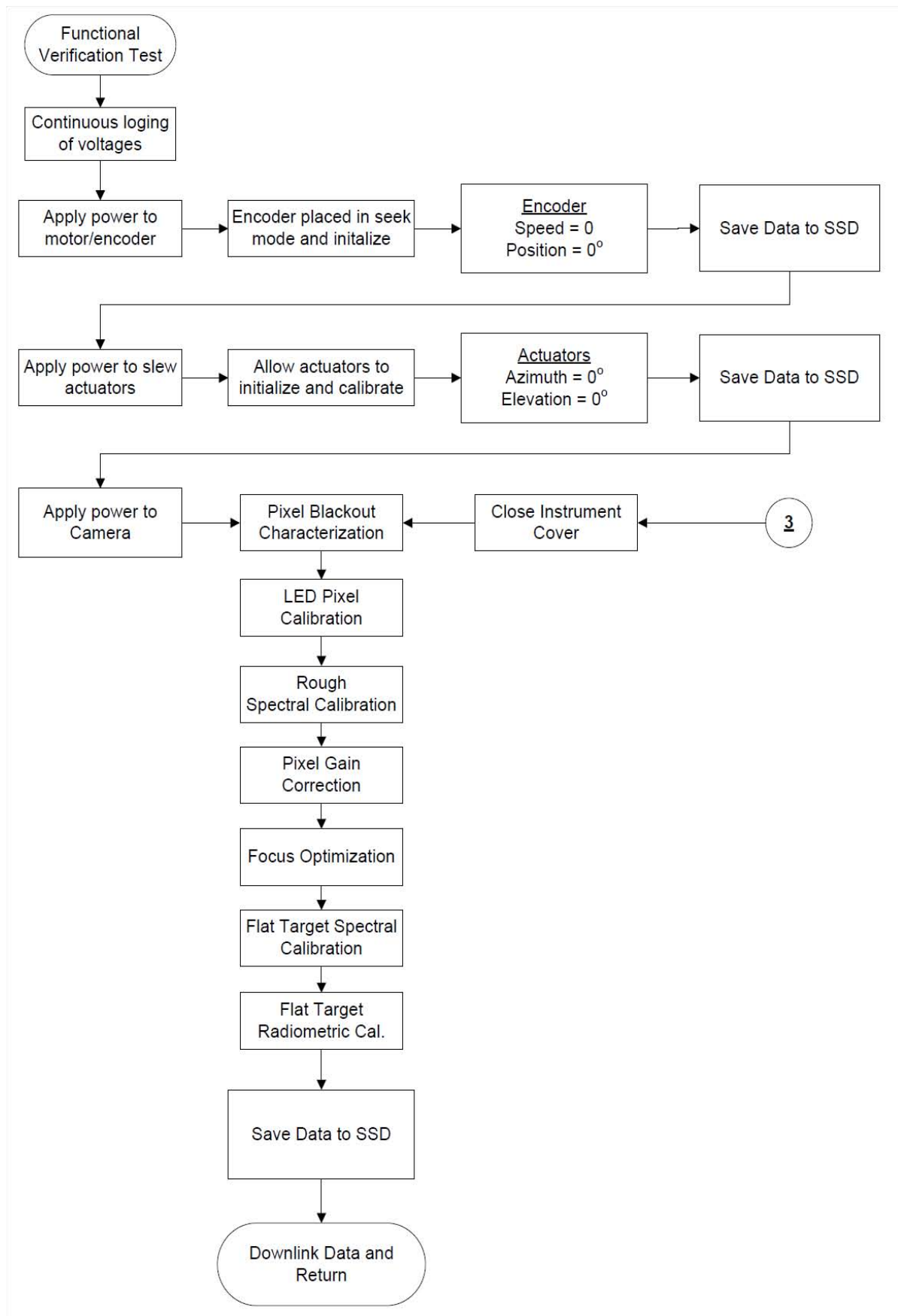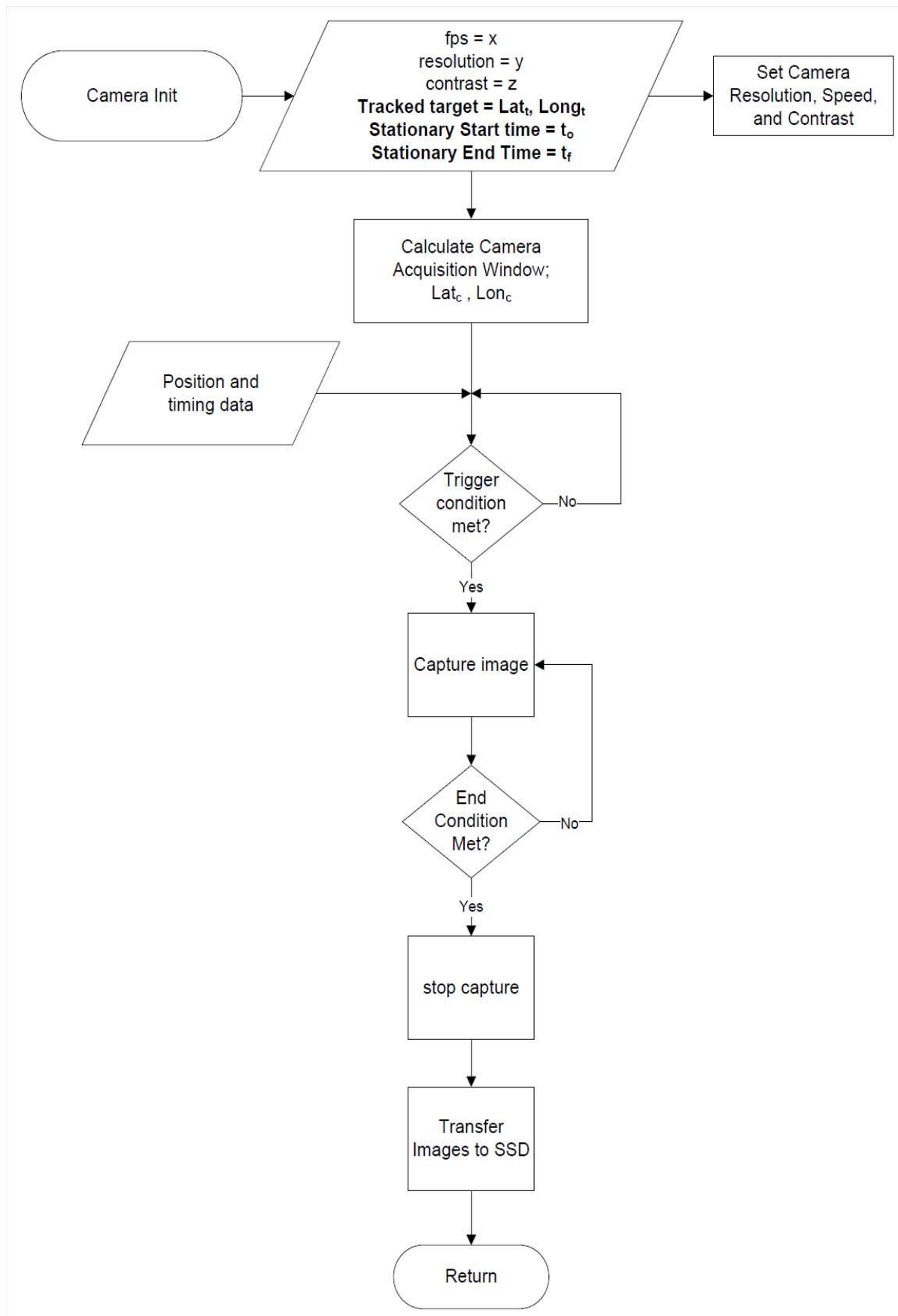
Figure C.2:   Function Verification

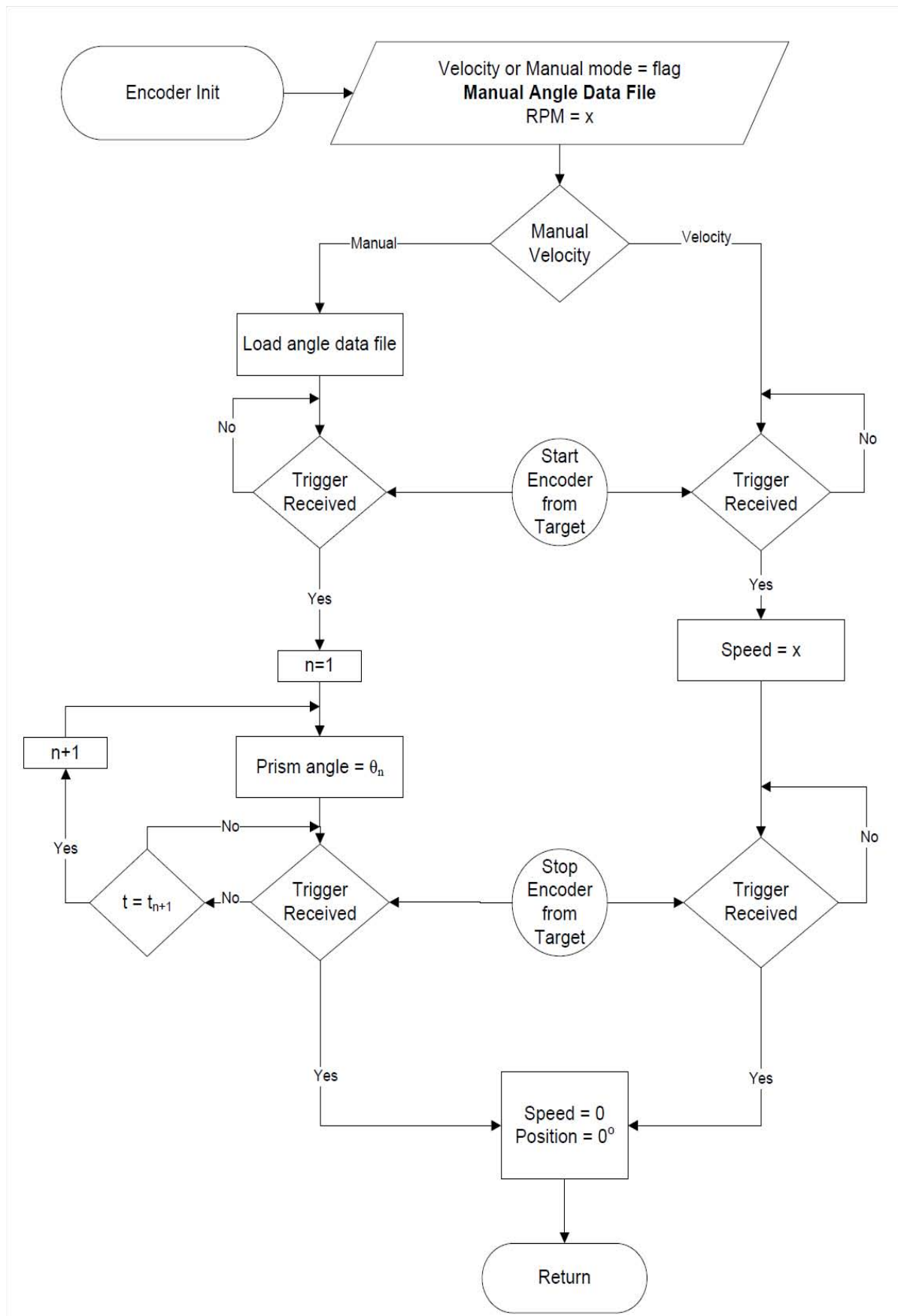Figure C.3:   Camera Initialization

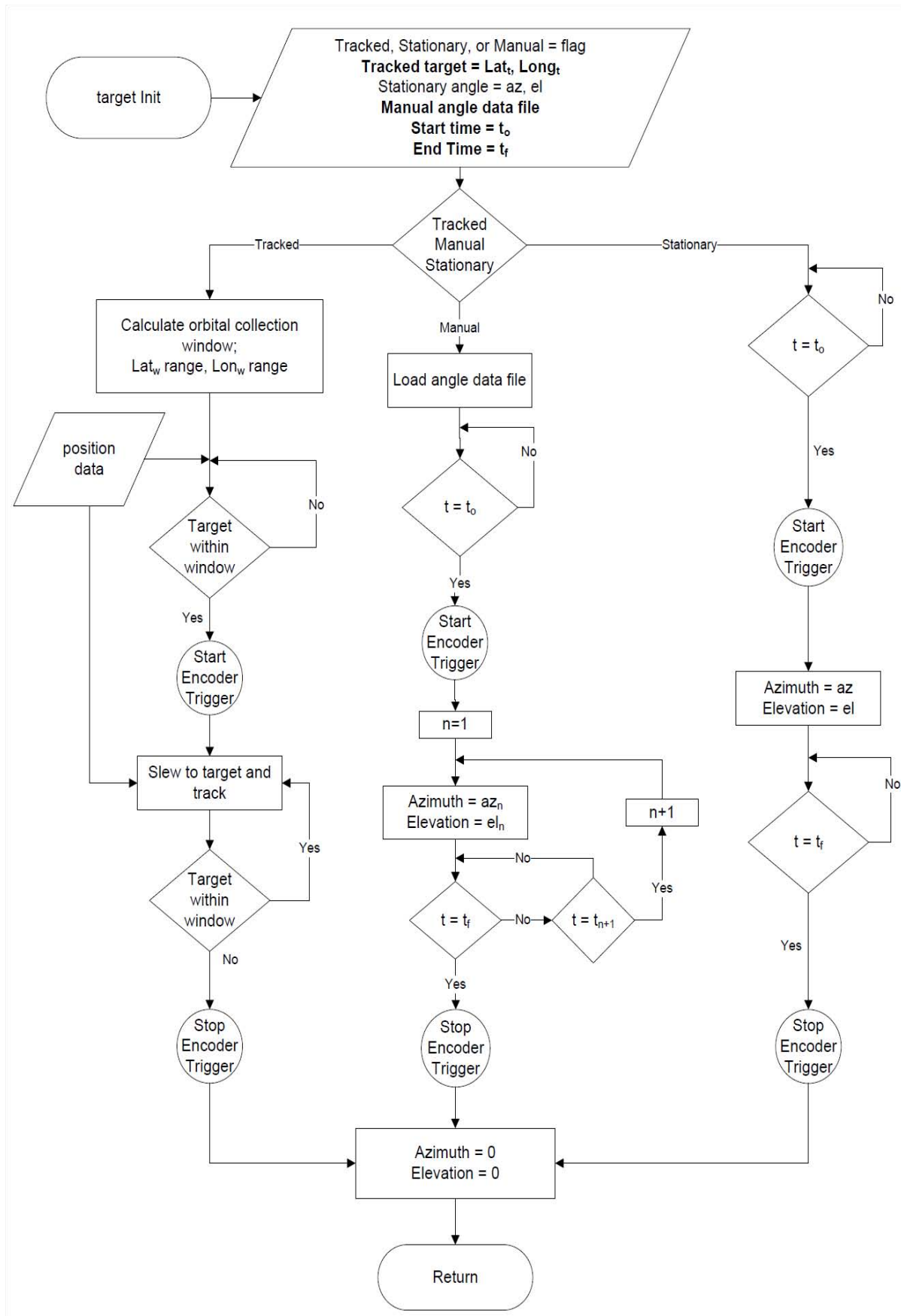Figure C.4:   Encoder Initialization

Figure C.5:   Data Collection Initialization

Bibliography

1. Vagni, F., "Survey of Hyperspectral and Multispectral Imaging Technologies," Tech. rep., ADA473675, NATO Research and Technology Organization, 2007.

2. "ADRS Series Mechanical-Bearing Rotary Stage," Tech. rep., Aerotech, 2009.

3. Morse, A., *Preliminary Electrical Designs for the CTEx Spacecraft and AFIT Satellite Ground Station*, Master's thesis, Air Force Institute of Technology, 2010.

4. Black, J. and Cobb, R., "Space Chromotomography Experiment (CTEx)," 2009, DOD Space Experiments Review Board Brief.

5. Smith, B. W., "Mapping the Spectrum: Techniques of Visual Representation in Research and Teaching Klaus Hentschel, Oxford University Press (2002)," *Spectrochimica Acta Part B: Atomic Spectroscopy*, Vol. 58, No. 3, 2003, pp. 581 – 582.

6. Grove, E. L., *Analytical Emission Spectroscopy*, Vol. I, Marcel Dekker, INC., New York, New York, 1971.

7. Beer, R., *Remote Sensing by Fourier Transform Spectroscopy*, John Wiley and Sons INC., New York, New York, 1992.

8. Arty, C., "Electromagnetic Spectrum," Available at http://www.colourtherapyhealing.com/colour/ images/electromagnetic-spectrum.jpg, 2007.

9. Garces, F. O., Available at http://faculty.sdmiramar.edu/fgarces/LabMatters/ Instruments/AA/Pic-AAS/specadd.jpg.

10. Lange, J., "Class Notes: OENG 533: Multispectral and Hyperspectral MASINT Exploitation," Winter Quarter 2007.

11. Short Sr., N. M., "The Remote Sensing Tutorial," Tech. rep., NASA, 2009, Available at http://rst.gsfc.nasa.gov/.

12. Bostick, R. L., Perram, G. P., and Tuttle, R., "Characterization of spatial and spectral resolution of a rotating prism chromotomographic hyperspectral imager," Vol. 7319, SPIE, 2009, p. 731903.

13. Mosher, T. and Mitchell, M., "Hyperspectral Imager for the Coastal Ocean (HICO)," *Aerospace Conference, 2004. Proceedings. 2004 IEEE*, Vol. 1, March 2004, pp. –28 Vol.1.

14. Corson, M., Korwan, D., Lucke, R., Snyder, W., and Davis, C., "The Hyperspectral Imager for the Coastal Ocean (HICO) on the International Space Station," *Geoscience and Remote Sensing Symposium, 2008. IGARSS 2008. IEEE International*, Vol. 4, July 2008, pp. IV –101–IV –104.

15. Corson, M., Bowles, J., Chen, W., Davis, C., Gallelli, K., Korwan, D., Lucey, P., Mosher, T., and Holasek, R., "The HICO Program - Hyperspectral Imaging of the Coastal Ocean from the International Space Station," *Geoscience and Remote Sensing Symposium, 2004. IGARSS '04. Proceedings. 2004 IEEE International*, Vol. 6, Sept. 2004, pp. 4184–4186 vol.6.

16. Mitchell, M. L., *Orbit Modeling of the International Space Station for Remote Sensing of Coral Reefs*, Master's thesis, Utah State University, 2006.

17. Clifford, G., "HICO/RAIDS Experiment Payload(HREP)," Tech. rep., Silver Engineering, 2009.

18. Ungar, S., Pearlman, J., Mendenhall, J., and Reuter, D., "Overview of the Earth Observing One (EO-1) mission," *Geoscience and Remote Sensing, IEEE Transactions on*, Vol. 41, No. 6, June 2003, pp. 1149–1159.

19. Pearlman, J., Barry, P., Segal, C., Shepanski, J., Beiso, D., and Carman, S., "Hyperion, a space-based imaging spectrometer," *Geoscience and Remote Sensing, IEEE Transactions on*, Vol. 41, No. 6, June 2003, pp. 1160–1173.

20. Pearlman, J., Carman, S., Segal, C., Jarecke, P., Barry, P., and Browne, W., "Overview of the Hyperion imaging spectrometer for the NASA EO-1 mission," *Proceedings. IGARSS*, Vol. 6, 2001, pp. 3504–3506.

21. Raymond, J., Stadter, P., Reed, C., Finnegan, E., Hurley, M., Merk, C., Kawecki, T., and Garner, C., "A TacSat Update and the ORS/JWS Standard Bus," *AIAA Fourth Responsive Space Conference*, Los Angeles, CA, April 24-27 2006.

22. Lockwood, R., Cooley, T., Nadile, R., Gardner, J., Armstrong, P., Payton, A., Davis, T., Straight, S., Chrien, T., Gussin, E., and Makowski, D., "Advanced Responsive Tactically-Effective Military Imaging Spectrometer (ARTEMIS) Design," *Geoscience and Remote Sensing Symposium, 2006. IGARSS 2006. IEEE International Conference on*, 31 2006-Aug. 4 2006, pp. 1628–1630.

23. Harlambakis, C., "Advanced Responsive Tactically Effective Military Imaging Spectrometer (ARTEMIS)," Fact sheet is available on the Raytheon website at http://www.raytheon.com-/capabilities/rtnwcm/groups/sas/documents-/content/rtn-sas-ds-artemis.pdf, 2009.

24. Troxel, I., Fehringer, M., and Chenoweth, M., "Achieving Multipurpose Space Imaging with the ARTEMIS Reconfigurable Payload Processor," *Aerospace Conference*, Big Sky, MT, March 1-8 2008.

25. Hatton, J., "The ISS as an Earth Observation Platform," Tech. rep., ESA/HSF-US, 2009.

26. Treder, A. J., "Space Station GN and C Overview for Payloads," *Space Technology and Applications International Forum-1999*, edited by M. El-Genk, AIP Conference Proceedings 458, American Institute of Physics, New York, 1999, pp. 49–57.

27. Frayman, R. and Strunce, R., "Spacecraft Slewing/Guidance Algorithm for Hyperspectral Imagers," AIAA, 2007.

28. Wertz, J. R. and Larson, W. J., *Space Mission Analysis and Design*, Microcosm Press, Hawthorne, CA, 3rd ed., 1999.

29. Bak, T., *Spacecraft Attitude Determination- a Magnetometer Approach*, Ph.D. thesis, Aalborg University, Denmark, 1999.

30. Liebe, C., "Star trackers for attitude determination," *Aerospace and Electronic Systems Magazine, IEEE*, Vol. 10, No. 6, Jun 1995, pp. 10–16.

31. Rabideau, G., Tran, D., Chien, S., Cichy, B., Sherwood, R., Mandl, D., Frye, S., Shulman, S., Szwaczkowski, J., Boyer, D., and Gaasbeck, J. V., "Mission Operations of Earth Observing-1 with Onboard Autonomy," *Second IEEE International Conference on Space Mission Challenges for Information Technology*, 2006.

32. Budzien, S., "RAIDS Update: The Remote Atmospheric and Ionospheric Detection System Aboard the ISS," Tech. rep., Naval Research Laboratory, September 9 2009.

33. Tech. rep.

34. Black, J., "Minimum Requirements For Space Imaging Component," Provided to RC Optics as the initial minimum design requirements for the telescope., 2008.

35. Book, T. A., *Design Analysis of a Space Based Chromotomographic Hyperspectral Imaging Experiment*, Master's thesis, Air Force Institute of Technology, 2010.

36. Hatton, J., "Call for Ideas Annex 1: Experiments for Global Climate Change from the ISS," Tech. rep., HSF-US/ESA-ESTEC, 2009.

37. de Boom, C., "Fine Sun Sensor," Tech. rep., TNO, 2009, Available at http://www.tno.nl/content.cfm?context=markten&content=case&laag1=191&item_id=1024.

38. de Boom, C., "Cosine Sun Sensor," Tech. rep., TNO, 2009, Available at http://www.tno.nl/content.cfm?context=markten&content=case&laag1=191&item_id=1023.

39. Budzien, S., "RAIDS Update: The Remote Atmospheric and Ionospheric Detection System Aboard the ISS," Tech. rep., Naval Research Laboratory, October 9 2009.

40. Dellinger, D., "Cloudiness-Mean Number of Days," Available at http://lwf.ncdc.noaa.gov/oa/climate/online/ccd/cldy.html, 2008.

REPORT DOCUMENTATION PAGE

Form Approved
OMB No. 0704–0188

1. REPORT DATE (DD–MM–YYYY)	2. REPORT TYPE	3. DATES COVERED (From — To)
25-03-2010	Master's Thesis	Jan 2009-Mar 2010

4. TITLE AND SUBTITLE	5a. CONTRACT NUMBER
Analysis of Slewing and Attitude Determination Requirements for CTEx	
	5b. GRANT NUMBER
	5c. PROGRAM ELEMENT NUMBER

6. AUTHOR(S)	5d. PROJECT NUMBER
Starr Jr., William J., MAJ, USA	
	5e. TASK NUMBER
	5f. WORK UNIT NUMBER

7. PERFORMING ORGANIZATION NAME(S) AND ADDRESS(ES)	8. PERFORMING ORGANIZATION REPORT NUMBER
Air Force Institute of Technology Graduate School of Engineering and Management (AFIT/ENY) 2950 Hobson Way WPAFB OH 45433-7765	AFIT/GSS/ENY/10-M05

9. SPONSORING / MONITORING AGENCY NAME(S) AND ADDRESS(ES)	10. SPONSOR/MONITOR'S ACRONYM(S)
Undisclosed Sponsor	
	11. SPONSOR/MONITOR'S REPORT

12. DISTRIBUTION / AVAILABILITY STATEMENT

APPROVED FOR PUBLIC RELEASE; DISTRIBUTION UNLIMITED

13. SUPPLEMENTARY NOTES

14. ABSTRACT

This thesis examines the slewing and attitude determination requirements for the Chromotomographic Experiment (CTEX), a chromotomographic-based hyperspectral imager, to be mounted on-board the Japanese Experiment Module (JEM) External Facility (EF). The in-track slewing requirement is driven by the facts that CTEx has a very small field of view (FOV) and is required to collect 10 seconds of data for any given collection window. The need to slew in the cross-track direction is a product of the small FOV and target/calibration site access. CTEx incorporates a two-axis slow-steering dwell mirror with a range of +/- 8 degrees and an accuracy of 10 arcseconds in each axis to slew the FOV. The inherent inaccuracy in the knowledge of the International Space Station's (ISS) attitude (+/- 3 degrees) poses significant complications in accurately pointing CTEx even with more accurate (0.3 degrees) attitude information provided by the JEM. The desire is for CTEx to incorporate a star tracker with 1 arcsecond accuracy to determine attitude without reliance on outside sources.

15. SUBJECT TERMS

Attitude Determination, Chromotomography, Chromotomographic Hyperspectral Imaging

16. SECURITY CLASSIFICATION OF:			17. LIMITATION OF ABSTRACT	18. NUMBER OF PAGES	19a. NAME OF RESPONSIBLE PERSON
a. REPORT	b. ABSTRACT	c. THIS PAGE	UU	97	Dr. Jonathan T. Black, AFIT/ENY
U	U	U			19b. TELEPHONE NUMBER (Include Area Code) (937)255-3636, ext 4578

Standard Form 298 (Rev. 8–98)
Prescribed by ANSI Std. Z39.18